Influence of mass on tarsus shape variation: a morphometrical investigation among Rhinocerotidae (Mammalia: Perissodactyla)

Cyril Etienne, Christophe Mallet, Raphael Cornette, Alexandra Houssaye

Influence of mass on tarsus shape variation: a morphometrical investigation among Rhinocerotidae (Mammalia: Perissodactyla)

Cyril Etienne[1*], Christophe Mallet[1], Raphaël Cornette[2], Alexandra Houssaye[1].

[1]UMR 7179, Mécanismes Adaptatifs et Evolution, Muséum National d'Histoire Naturelle, Centre National de la Recherche Scientifique, Paris, France.

[2]UMR 7205, Institut de Systématique, Evolution, Biodiversité, Centre National de la Recherche Scientifique, Muséum National d'Histoire Naturelle, Université Pierre et Marie Curie, Ecole Publique des Hautes Etudes, Paris, France.

*Corresponding author. E-mail: cyril.etienne@cri-paris.org

Running title: Influence of mass on tarsus shape in Rhinocerotidae.

Abstract

Many tetrapod lineages show extreme increases in body mass in their evolutionary history, associated with important osteological changes. The ankle joint, essential for foot movement, is assumed to be especially affected. We investigated the morphological adaptations of the astragalus and the calcaneus in Rhinocerotidae, and analysed them in light of a comparative analysis with other Perissodactyla. We performed 3D geometric morphometrics and correlated shape with centroid size of the bone and body mass of the species. Our results show that mass has an influence on bone shape in Rhinocerotidae and in Perissodactyla, but not as strong as expected. In heavy animals the astragalus has a flatter trochlea, oriented more proximally, associated with a more upright posture of the limb. The calcaneus is more robust, possibly to sustain the greater tension force exerted by the muscles during plantarflexion. Both bones show wider articular facets, providing greater cohesion and better dissipation of the loading forces. The body plan of the animals also has an influence. Short-legged Teleoceratina show a flatter astragalus than the other rhinocerotids. *Paraceratherium* has a thinner calcaneus than expected. This study clarifies adaptations to heavy weight among Rhinocerotidae and calls for similar investigations in other groups with massive forms.

Key words: ankle - astragalus - calcaneus - functional morphology - heavy weight – geometric morphometrics - Perissodactyla – Rhinocerotidae

Introduction

In vertebrate locomotion, bone is a rigid organ of paramount importance. It provides support for the body as well as attachment points for the muscles, via the tendons (Hildebrand, 1982; Biewener, 1990). Bone shape varies with a diversity of factors, one of the main ones being the size of the animal (Hildebrand *et al.*, 1985; Biewener, 1989; Polly, 2008; Biewener & Patek, 2018). Evolutionary convergences are usually observed when similar selective pressures are applied to the same structure independently in different groups. Accordingly, in a given clade, an increasing mass generally results in *e.g.* a more vertical orientation of the pelvis (Polly, 2008), an increasing diameter of the femur (Alexander, 1985), and micro-anatomical changes such as a high thickness of cortical bone (Houssaye *et al*., 2016). Postural and locomotor factors such as facultative bipedalism or cursoriality are also important factors influencing the shape of the skeleton, (Hildebrand, 1982; Polly, 2008). Analysing the relationship between mass and the shape of the bones, while considering also factors such as posture and locomotion, would allow a better understanding of the way animals with different body plans adapt to an increasing mass.

Rhinocerotidae (Gray, 1821) seem to be an excellent group to study morphological variations in bone related to mass and to a varying body plan. Today comprising five species and four genera, rhinocerotids are found only in tropical regions (Dinerstein, 2011). They were much more diverse during the Cenozoic, appearing in the middle of the Eocene and comprising more than a hundred species (Cerdeño, 1998). Rhinocerotids have been found in Eurasia, Africa and North America (as far south as Panama; MacFadden [2006]), and existed in a diversity of habitats, e.g. cold steppes, dense forests or swamps (Prothero *et al*., 1989; Mörs, 2002; Prothero, 2005). All of them were relatively heavy animals as compared to the average body mass of mammals (Gardezi & da Silva, 1999), ranging from approximately 150 kg for the lightest taxa of the Eocene to five tons for *Elasmotherium* (Cerdeño, 1998; Becker, 2003; Antoine in press). They showed several independent extreme increases of body mass, up to more than two tons, during their evolutionary history (e.g. in Rhinocerotina, Teleoceratina or Elasmotheriinae; Cerdeño, 1998). They also vary in terms of body plan: some taxa are massive and sturdy (e.g. *Coelodonta*, *Ceratotherium*), some are extremely short-legged (e.g. *Teleoceras*, *Brachypotherium, Prosantorhinus* in the Teleoceratina tribe), others have been described as gracile and cursorial (e.g. *Protaceratherium*, *Hispanotherium*, Cerdeño, 1998). Rhinocerotids should therefore be a very interesting group to study bone shape variations, and analyse its relationship with different masses and morphologies. Rhinocerotidae are part of the order

Perissodactyla (Owen, 1848). If they nowadays only include the five species of Rhinocerotidae, the seven species of Equidae and the four species of Tapiridae, they were much more diversified during the Cenozoic, in terms of number of species and families (Prothero & Schoch [1989], see figure 1). They included notably the Paraceratheriidae (sometimes considered a subfamily of Hyracodontidae, see Wang *et al.*, 2016), which included some of the heaviest land mammals that ever lived (Prothero, 2013). Perissodactyla also included the intriguing Chalicotheriidae, among which some species (the subfamily Chalicotheriinae) were facultative bipeds with a gorilla-like stance, with very short hindlimbs and walking on the knuckles of their forelimbs, whereas others (the Schizotheriinae) had front and hindlimbs of approximately equal length (Coombs, 1983; Semprebon *et al.*, 2011). This order therefore encompasses a great diversity in terms of mass and body plan that can be related to their bone shape, and compared with the diversity observed among Rhinocerotidae.

Our study focused on two bones of the tarsus: the astragalus and the calcaneus. These bones are at the junction between the hind zeugopodium and the autopodium, and are essential to the movement of the foot and consequently of the entire animal. The astragalus serves as the pivot, or fulcrum, and the calcaneus as the lever arm of the foot (Carrano, 1997). These bones have been extensively studied, from taxonomic and phylogenetic points of view (see Gladman *et al*., 2013; Guérin, 1980; Missiaen *et al*., 2006; Stains, 1959), but also in a morphofunctional context, with multiple studies trying to link their shape to the animal's mass (see Dagosto & Terranova, 1992; Martinez & Sudre, 1995; Tsubamoto, 2014), habitat (DeGusta & Vrba, 2003; Plummer *et al*., 2008; Curran, 2012; Barr, 2014), and mode of locomotion (Nakatsukasa *et al.*, 1997; Panciroli *et al.*, 2017). These studies all found a link between the mass of a species and the shape of its astragalus and of its calcaneus, generally represented by linear measurements or ratios. These studies concerned a great variety of mammals, e.g. bovids, cervids, carnivorans, primates, but none ever specifically studied the relationship between mass and shape on both ankle bones in perissodactyls.

In the present study, we investigated the variation of the shape of the astragalus and calcaneus across a diversity of extant and fossil Rhinocerotidae and additional Perissodactyla. Our primary aim was to identify shape variations associated with an increase of mass. We expect that mass will have a strong influence on those bones since they are extremely important for the support and movement in mammals. We expect that bones of large animals will be more robust and more resistant, with wider and flatter articular facets to help dissipate forces. We also expect that adaptations will vary according to the general body plan and mode of

locomotion of the animal. We studied variations of bone shape, and tested the influence of the bone size and of the mean mass of each species. We first focused on shape variations across Rhinocerotidae, and then across all Perissodactyla sampled in order to compare the variations observed among Rhinocerotidae to more diverse forms (e.g. *Paraceratherium*), and thus better interpret the drivers acting on this variation.

Material and methods

Material

We studied 112 astragali and 94 calcanei belonging to 43 different species across five different families of Perissodactyla, with varying masses, morphologies or locomotor modes (Appendix 1; Fig. 1). Taxa were chosen in order to encompass as much as possible of the variation within Rhinocerotidae. A few specimens of other families of Perissodactyla with particular characteristics (e.g. an extremely high mass for *Paraceratherium*, cursoriality for horses, shortened hindlimbs for Chalicotheriinae) were included to provide a comparison point for the shape variations observed in Rhinocerotidae. Rhinocerotidae constitutes our main subsample, with 40 specimens of each bone type for living species. Our sample also includes 43 astragali and 31 calcanei of fossil Rhinocerotidae, including small, cursorial genera (*Protaceratherium*, *Pleuroceros*), and at least three lineages presenting independent rises of body mass above two tons (in *Elasmotherium*, *Brachypotherium*, *Coelodonta*, plus the living *Ceratotherium* and *Rhinoceros unicornis*). We studied 10 astragali and calcanei of extant Tapiridae, and eight astragali and six calcanei of Equidae. Three astragali and one calcaneus belong to *Paraceratherium* (Paraceratheriidae), and eight astragali and six calcanei belong to Chalicotheriidae. To our knowledge, all the bones belonged to adult specimens. A description of the bones including the nomenclature used for the main anatomical features of the bones is provided in Appendix 2.

Specimens come from the collections of the Muséum National d'Histoire Naturelle (MNHN, Paris, France), the Muséum d'Histoire Naturelle de Toulouse (MHNT, Toulouse, France), the Claude Bernard University (UCBL, Lyon, France), the Natural History Museum (NHM, London, United Kingdom), the Powell-Cotton Museum (BICPC, Birchington-on-Sea, United Kingdom), the Naturhistorisches Museum Wien (NMW, Vienna, Austria), the Zoologische Staatssammlung München (ZSM, Munich, Germany), and the Bayerische Staatssammlung für Paläontologie und Historiche Geologie (BSPHM, Munich, Germany; Appendix 1).

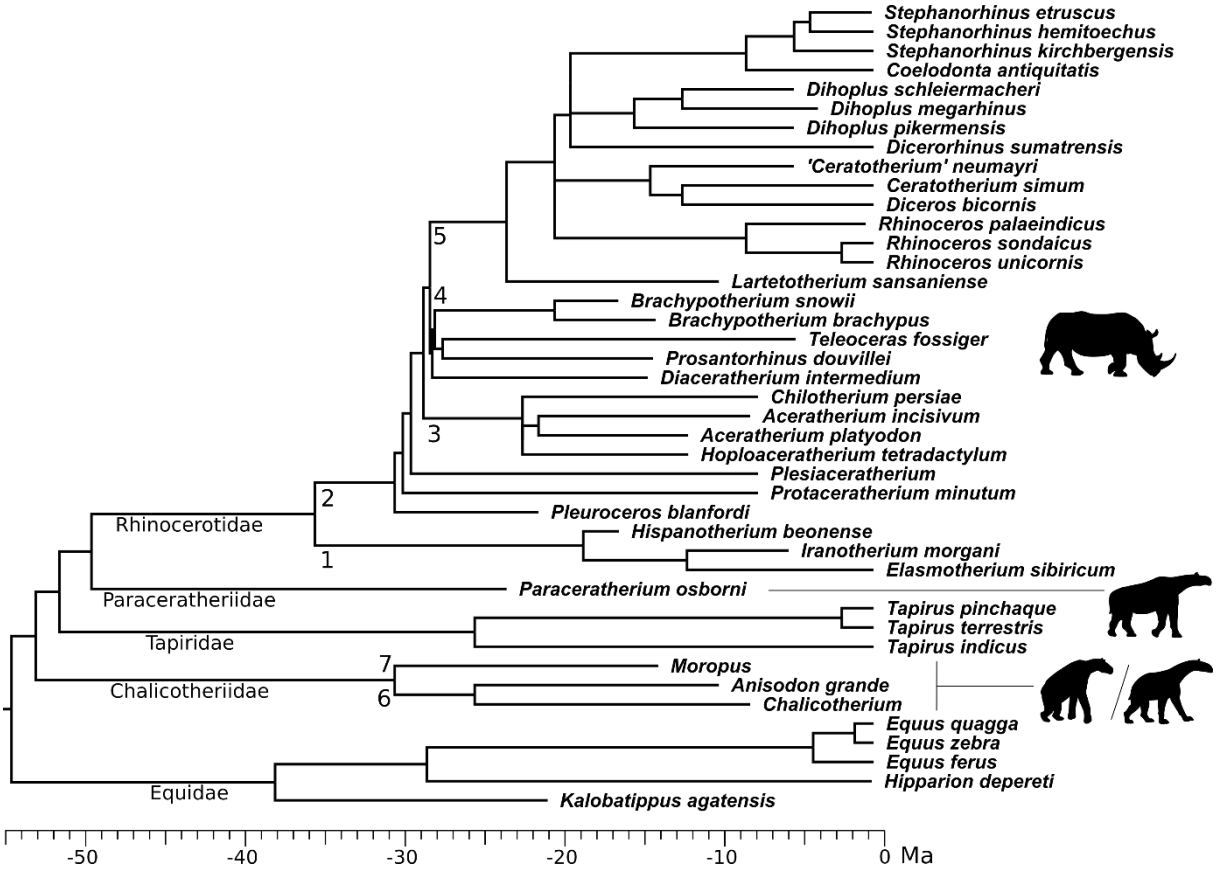

Fig. 1. Composite phylogeny including the species sampled, modified from Antoine, 2002, Antoine *et al.*, 2010, Antoine *et al.* in press, Holbrook and Lapergola, 2011, Piras *et al.*, 2010 and Steiner and Ryder, 2011. Occurrence dates were estimated using Antoine, 1997, Piras *et al.*, 2010, Antoine *et al.*, 2010, Geraads *et al.*, 2012, Guérin, 2012, and Prothero, 2013, as well as data recorded on http://fossilworks.org. 1: Elasmotheriinae; 2: Rhinocerotinae; 3: Aceratheriina; 4: Teleoceratina; 5: Rhinocerotina; 6: Schizotheriinae; 7: Chalicotheriinae. Species in bold are living species. The relationships between the five extant rhino species are still debated, specifically the position of *Dicerorhinus sumatrensis* and its close fossil relatives is uncertain, placed either as sister taxa to *Ceratotherium* and *Diceros*, as sister taxa to *Rhinoceros*, or as sister taxa to a group formed of *Rhinoceros*, *Ceratotherium* and *Diceros* (Willerslev *et al.*, 2009; Gaudry, 2017). This phylogenetic uncertainty is here represented by a polytomy.

Mass estimations used

Mass data were retrieved from the literature (Table 1). Methods of mass reconstructions are detailed in the references; they usually relied on regression equations and measurements on the molars or on proximal limb segments. None of them used measurements on the astragalus or the calcaneus. When only a range of masses was available with no average, the mean of the minimal and maximal mass was used.

Table 1. List of the masses used for the species studied here. †: fossil taxon. *: two separate mass estimates were used for *Equus caballus*, one for average-sized horses and one for draught horses, given the wide morphological differences between the two.

Family	Species	Mass (kg)	Source
Rhinocerotidae	*Rhinoceros sondaicus*	1200-1500	Dinerstein, 2011
Rhinocerotidae	*Rhinoceros unicornis*	2000	Dinerstein, 2011
Rhinocerotidae	*Rhinoceros palaeindicus* †	Missing data	
Rhinocerotidae	*Diceros bicornis*	800-1300	Dinerstein, 2011
Rhinocerotidae	*Ceratotherium neumayri* †	1200	Valli, 2005
Rhinocerotidae	*Ceratotherium simum*	2300	Dinerstein, 2011
Rhinocerotidae	*Dicerorhinus sumatrensis*	600-950	Dinerstein, 2011
Rhinocerotidae	*Stephanorhinus etruscus* †	Missing data	
Rhinocerotidae	*Stephanorhinus kirchbergensis* †	1844	Saarinen *et al.,* 2016
Rhinocerotidae	*Stephanorhinus hemitoechus* †	Missing data	
Rhinocerotidae	*Coelodonta antiquitatis* †	1905	Saarinen et al., 2016
Rhinocerotidae	*Dihoplus megarhinus* †	Missing data	
Rhinocerotidae	*Dihoplus schleiermacheri* †	1812	Becker, 2003
Rhinocerotidae	*Dihoplus pikermensis* †	1100	Valli, 2005
Rhinocerotidae	*Lartetotherium sansaniense* †	1204	Becker, 2003
Rhinocerotidae	*Prosantorhinus douvillei* †	Missing data	
Rhinocerotidae	*Teleoceras fossiger* †	1016	Damuth, 1990
Rhinocerotidae	*Brachypotherium brachypus* †	2327	Becker, 2003
Rhinocerotidae	*Brachypotherium snowi* †	Missing data	
Rhinocerotidae	*Aceratherium incisivum* †	1982	Becker, 2003
Rhinocerotidae	*Aceratherium platyodon* †	Missing data	
Rhinocerotidae	*Hoploaceratherium tetradactylum* †	1197	Becker, 2003
Rhinocerotidae	*Chilotherium persiae* †	Missing data	
Rhinocerotidae	*Diaceratherium intermedium* †	Missing data	
Rhinocerotidae	*Plesiaceratherium* †	Missing data	
Rhinocerotidae	*Protaceratherium minutum* †	530	Becker, 2003
Rhinocerotidae	*Pleuroceros blanfordi* †	501	Becker, 2003
Rhinocerotidae	*Victoriaceros kenyensis* †	Missing data	
Rhinocerotidae	*Hispanotherium beonense* †	Missing data	
Rhinocerotidae	*Elasmotherium sibiricum* †	4000-5000	Zhegallo *et al.,* 2005
Rhinocerotidae	*Iranotherium morgani* †	Missing data	
Paraceratheriidae †	*Paraceratherium bugtiense* †	7400	Fortelius & Kappelman, 1993
Tapiridae	*Tapirus pinchaque*	150-200	Medici, 2011
Tapiridae	*Tapirus terrestris*	220	Medici, 2011
Tapiridae	*Tapirus indicus*	280-400	Medici, 2011
Chalicotheriidae †	*Chalicotherium sp.* †	924	Costeur, 2004
Chalicotheriidae †	*Anisodon grande* †	1500	Guérin, 2012
Chalicotheriidae †	*Moropus sp.* †	1179	Damuth, 1990
Equidae	*Equus zebra*	240-380	Rubenstein, 2011
Equidae	*Equus quagga*	175-320	Rubenstein, 2011
Equidae	*Equus przewalski*	200-300	Rubenstein, 2011
Equidae	*Equus caballus*	380-600	Bongianni, 1988

Equidae	*Equus caballus* *	700-1000	Bongianni, 1988
Equidae	*Hipparion depereti* †	Missing data	
Equidae	*Kalobatippus agatensis* †	160	Jams et al., 1994

Data acquisition

The specimens were digitized using either an Artec Eva surface scanner and the Artec Studio Professional v12.1.5.1 software (Artec 3D, 2018), or a Nikon D5500 camera (automatic mode, without flash, focal length 50 mm, aperture f/1.8) and the photogrammetry software Agisoft PhotoScan v1.4.0 (Agisoft LLC, 2017). The 3D meshes were then exported, decimated down to 60,000 faces and mirrored to have only right side astragali and calcanei, using MeshLab v2016.12 (Cignoni *et al.*, 2008). In two cases (The astragalus of *Brachypotherium snowi* NHM-PAL-PV-M-29279 and the calcaneus of *Hispanotherium beonense* MHNT-2015-0-837), the specimens were slightly damaged where a curve would pass and had to be partially reconstructed using Geomagic (3D Systems, 2017).

Geometric morphometrics

Bone shape was modelled using anatomical landmarks and semi-landmarks sliding on curves (Gunz & Mitteroecker, 2013). Landmarks were all placed by the same operator (C.E.). Given that there can be marked differences in bone shape between rhinocerotids and the other perissodactyls, we split the analysis in two. Two sets of landmarks and curves were therefore defined: one for all the rhinocerotids, and another for all the perissodactyls (see Figs. 2, 3; Appendix 3 for descriptions of the landmarks and curves), with fewer landmarks and curves but able to encompass a broader number of taxa. The second set is mostly a subset of the first one, only two curves had to be redefined. Landmarks and curves were digitized on the meshes using the IDAV Landmark software package (Wiley, 2005). All the analyses and statistical tests were run using R (R Development Core Team, 2005) and RStudio (RStudio, Inc., 2018). The curves were resampled using the algorithm provided in Botton-Divet *et al.* (2016). Then, as the algorithm can result in some semi-landmarks being slightly above or below the mesh surface, the semi-landmarks were reprojected on the meshes using the closemeshKD function of the Morpho R package (Schlager *et al.*, 2018), which uses the coordinates of each semi-landmark to calculate its closest match on the surface of the mesh.

Landmarks were superimposed using a Generalized Procrustes Analysis (GPA), which translates, scales and rotates each set of landmarks in order to remove the information of size,

position and angle, and to minimize the sum of square distances between landmark configurations (Bookstein, 1991). The curve semi-landmarks were slid along the curves in order to minimize the bending energy of a Thin-Plate-Spline as described in Gunz *et al.* (2005). The bending energy is a scalar quantity that roughly represents the amount of local shape deformation between a reference set of landmarks (chosen arbitrarily among our sample). More technically, it is the integral of the squared second derivatives of the deformation (see Gunz and Mitteroecker, 2013; Mitteroecker and Gunz, 2009).

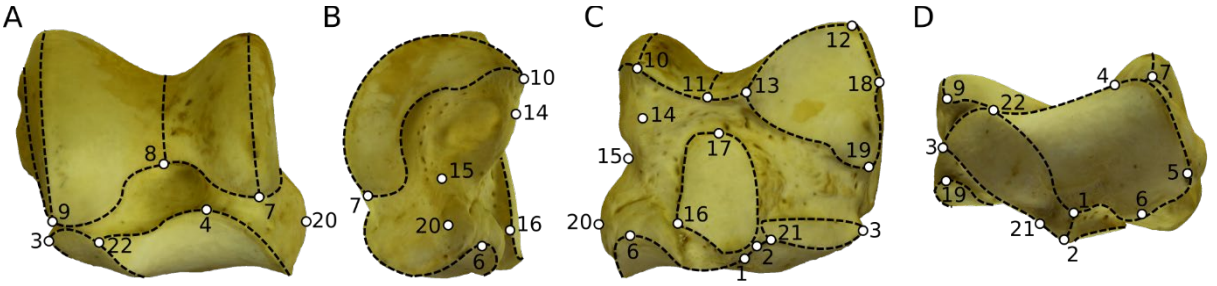

Fig. 2. Representation of the landmarks and the curves placed on the astragalus of *Rhinoceros unicornis* MNHN-ZM-AC-1960-59. A: anterior, B: medial, C: posterior and D: distal views. White dots denote the 22 anatomical landmarks, dotted black lines the 9 curves. Description of the landmarks and curves is provided in Appendix 3.

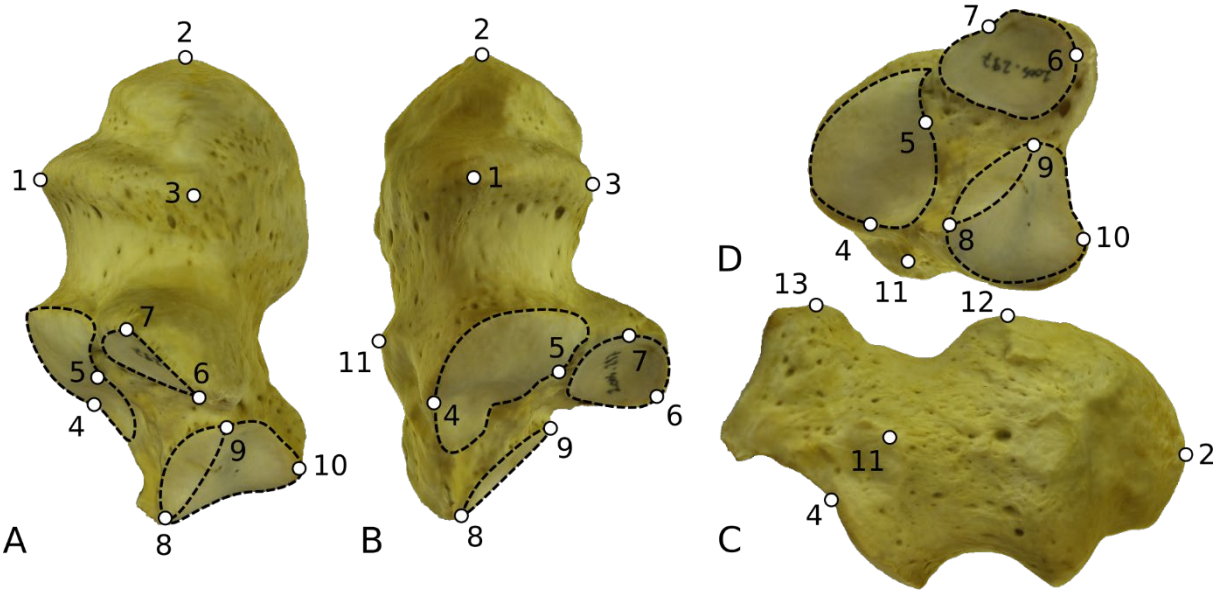

Fig. 3. Representation of the landmarks and curves placed on the calcaneus of *Ceratotherium simum* MNHN-ZM-MO-2005-297. A: medial, B: anterior, C: latero-anterior and D: distal views. White dots denote the 13 anatomical landmarks, dotted black lines the 4 curves. Description of the landmarks and curves is provided in Appendix 3.

To assess the repeatability of the landmarks, and prior to placing the landmarks on the whole sample, we placed each landmark ten times on each of three specimens of *Diceros bicornis*, alternating between each specimen. The three specimens were assessed by sight to be the three morphologically closest. These 30 landmark sets were then superimposed using a Generalized Procrustes Analysis and visualized using a Principal Components Analysis (PCA), to check that landmark error per specimen was smaller than inter individual variation (Appendix 4).

Statistical analyses

After the GPA, the aligned landmarks coordinates were used in a PCA, in order to reduce dimensionality of our data and assess the shape variation patterns in our sample. Neighbour-Joining trees were generated using a Euclidian distance matrix based on the PC-scores, in order to visualize the phenotypic similarities between each specimen or group in a multivariate manner, instead of one axis at a time, which is useful if each axis explains a small percentage of variance. PC-scores were used instead of Procrustes coordinates to reduce number of dimensions and thus lower the computing power required.

We tested the influence of the centroid size of each bone on its shape. Centroid size is defined as the square root of the sum of the square of the distance of each point to the centroid of the landmark set; it is most commonly used to assess the variations of shape that are due to variations of size, or allometry (Mitteroecker *et al.*, 2013; Klingenberg, 2016). Logarithms were used for the centroid size values, as recommended by Bookstein (1991) and Klingenberg (1996). Procrustes coordinates were correlated against centroid size using a multivariate regression. The allometry-free residuals from the tests were used to create allometry-free shapes for each individual, allowing analyses where the influence of size is entirely removed (see e.g. Evin *et al*., 2011; Perrard *et al.*, 2012).

The centroid size of both bones is statistically linked to the mean mass of the species in our sample (see Appendix 5; $p < 0.0001$, R^2 between 0.46 and 0.82 depending on the bone and the landmark set). The R-square is however different from 1, therefore mass could have an influence on the shape of the bones that is independent from its centroid size. For example, two astragali or calcanei with the same centroid size belonging to species with different mean masses would exhibit divergent shapes. This was tested using a multivariate regression of the allometry-free shapes generated earlier on the logarithm of the cubic root of the mean mass of the species. Given that we could not find mass estimation for 14 sampled species, they have been removed from this analysis.

In order to assess what the effect of shared evolutionary history of different species is on the shape of the astragalus and calcaneus, the degree of phylogenetic signal in the morphological data was also assessed, using a multivariate K statistic (K-mult) based on the PC-scores. It compares the observed rate of morphological change to the expected change under a Brownian motion (see Adams, 2014; Blomberg *et al.*, 2003). The phylogeny used is provided in figure 1. Results are provided in Appendix 6.

Thin Plate Splines were used to visualize the results of our analyses: for each set of landmarks on the calcaneus and astragalus, the mean-shape generated by the GPA was mapped onto the specimen closest to the mean value. Then, this mean-shaped model was deformed towards the shape resulting from our analyses, for instance the shape extremes of each PCA axis.

Results

Rhinocerotidae

Astragalus

Morphological variations

The Neighbour-Joining tree (Fig. 4) generally shows a greater morphological proximity between members of the same species than between members of different species, which indicates that interspecific variation is generally greater than intraspecific variation. The Teleoceratina, the short-legged rhinocerotids, are clearly grouped and separated from the others, except *Diaceratherium*. Among them, *Teleoceras* has a very long branch indicating a very derived morphology for this individual. *Dicerorhinus*, *Ceratotherium simum* and *Rhinoceros* all form homogenous groups, but *Diceros* has two specimens that are separated from the others. This might be due to them possibly belonging to different subspecies or a different sex, but this is unknown for these specimens. All the fossil dicerorhinins (*Dihoplus*, *Stephanorhinus* and *Coelodonta*) are grouped together, but *Dicerorhinus sumatrensis* is separated from them. Aceratheriina, Elasmotheriinae, *Diaceratherium*, *Protaceratherium*, *Pleuroceros,* and *Plesiaceratherium* tend to all group together, with a few exceptions. The two specimens of *Iranotherium morgani* are clearly separated from one another in the tree; this is also the case for the two *Ceratotherium neumayri* specimens. Above the tribe level, there are no clusters that seem to follow the phylogeny.

A low percentage of variance is explained by each axis of the PCA on Rhinocerotidae astragali (63.1% for the first ten axes). Only the principal components that are correlated to centroid size, or that highlight variations of shape that could be due to differences in terms of animal general body plan, are described. Thus, only PC1, PC2 and PC4 are described here. PC1 highlights differences in astragalus shape between species with different morphologies, PC2 and PC4 are weakly but significantly correlated with centroid size. PC2 is positively correlated with centroid size ($p < 0.001$, $R^2 = 0.17$), and PC4 is negatively correlated with centroid size ($p < 0.001$, $R^2 = 0.12$). Vector representations of the deformations along the principal components are provided in Appendix 7.

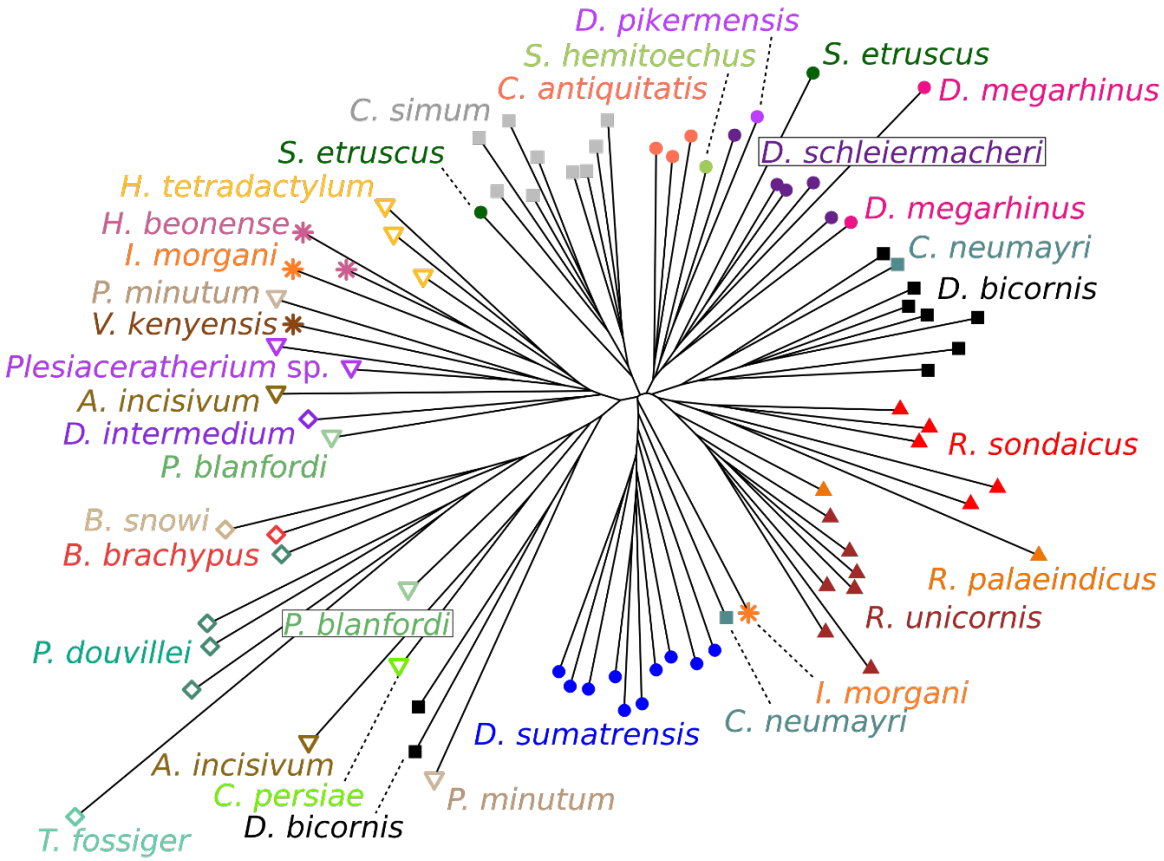

Fig. 4. Neighbour-Joining tree generated from a matrix of the Euclidian distance between every specimen, on the astragali of Rhinocerotidae. Legend as in Fig. 5.

PC1 (14.2% of variance, Fig. 5) strongly separates members of the short-legged Teleoceratina, on the negative side, from the other Rhinocerotidae. The axis is characterized in its negative extremity by a great proximo-distal compression of the bone; a flatter and symmetrical trochlea with medio-laterally wider and lower ridges; and a trochlea with a more proximal than anterior orientation. As for the articular facets, in the negative side of the PC1 the proximal facet with the calcaneus is distally elongate; the medial facet for the calcaneus is proximo-distally compressed, twice as broad (medio-laterally) as high (proximo-distally), and not fused with the distal facet; the distal facet for the calcaneus is medio-laterally very short; and the facet for the navicular is broader than on the positive extremity of the axis, covering most of the distal face of the astragalus.

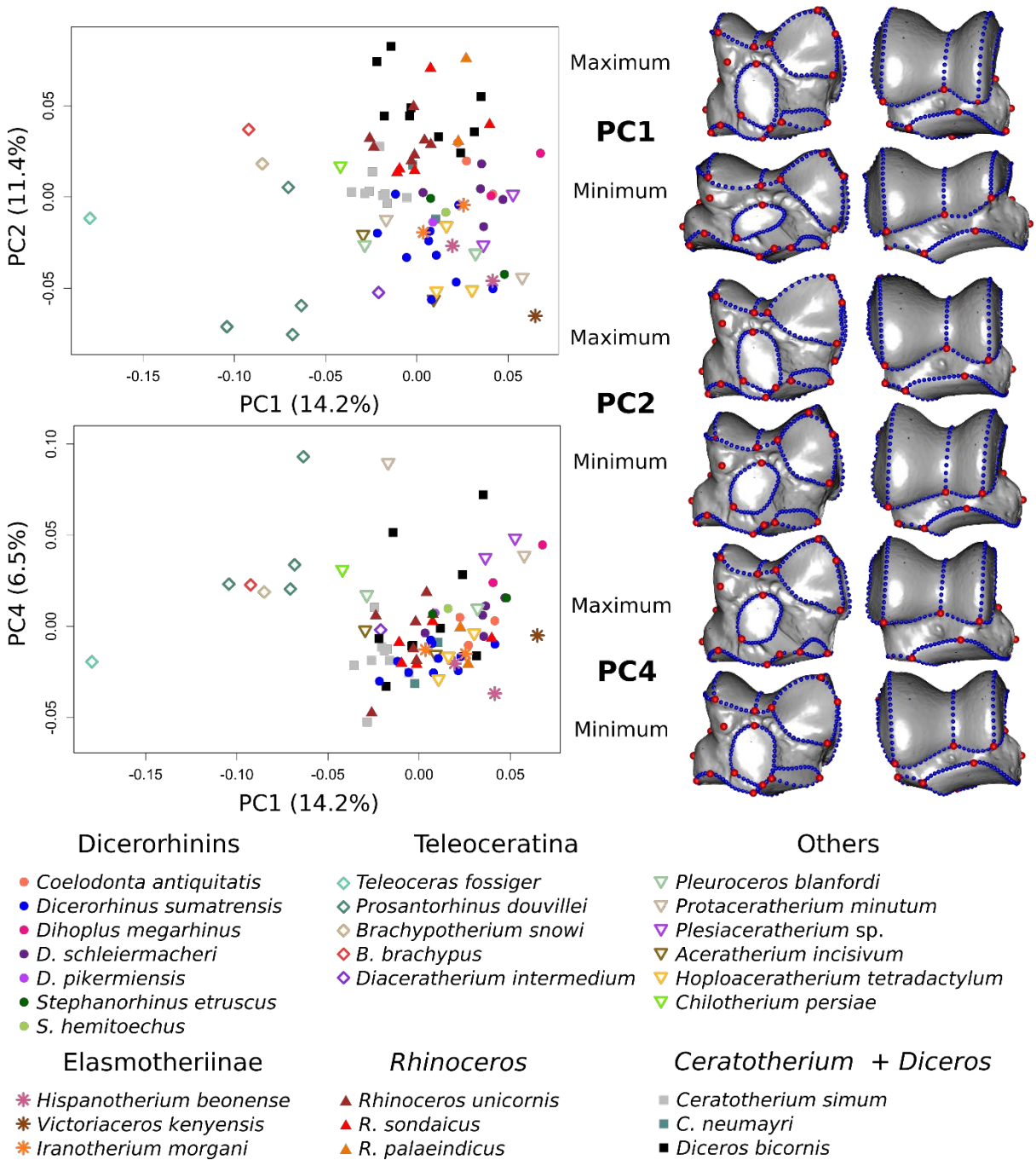

Fig. 5. Results of the PCA performed on the astragalus of Rhinocerotidae. Left: repartition of the Rhinocerotidae astragali studied across PC1, PC2 and PC4. Right: TPS deformation of a mean shape towards the maximal and minimal value of each axis. The view is first posterior then anterior. Red dots denote landmarks, blue dots denote curve semi-landmarks. Vector representations of the deformations are provided in Appendix 7A.

Along PC2 (11.4% of variance, Fig. 5), *Diceros*, *Rhinoceros* and *Brachypotherium* are placed on the positive side, and *Dicerorhinus*, *Hoploaceratherium*, *Aceratherium*, *Hispanotherium* and *Victoriaceros* on the negative side, the other genera being scattered around

the centre. Teleoceratina are spread across the whole axis. The axis is characterized in its negative extremity by a higher lateral ridge of the trochlea than observed on the positive side; a less concave distal contour of the trochlea; the pentagonal shape of the proximal facet for the calcaneus, in contrast with the medio-laterally wider triangular shape observed on the positive side; and a proximo-distal shortening of the medial facet for the calcaneus, which does not reach the distalmost point of the bone as it does on the positive side.

PC4 (6.5% of variance, Fig. 5) shows *Protaceratherium*, *Plesiaceratherium* and *Prosantorhinus* on the positive part of the axis, and *Hispanotherium*, *Iranotherium*, *Hoploaceratherium*, *Ceratotherium*, *Dicerorhinus* and *Teleoceras* on the negative part. It is characterized in its negative extremity by a very short neck of the astragalus; a more proximal orientation of the trochlea; a distal shortening of the proximal facet for the calcaneus; and a fusion of the medial and distal facets for the calcaneus, whereas both are very well separated on the positive part of the axis.

Impact of allometry and mass

The centroid size has a significant but weak effect on the shape of the astragalus ($p < 0.01$ and $R^2 = 0.04$, according to multivariate regression of the logarithm of the centroid size on the Procrustes coordinates). A large astragalus (Fig. 6A) is characterized by a medio-laterally wider and triangle-shaped proximal facet with the calcaneus; medio-laterally wider and fused medial and distal facets with the calcaneus; and an articular facet with the navicular positioned less laterally offset, more directly underneath the rest of the bone.

Once the influence of the centroid size is removed, there is only a weak influence of the mass of the species on the shape of the astragalus ($p < 0.05$, $R^2 = 0.03$). The shape variations are minimal: in an astragalus pertaining to a heavy species (Fig. 6B), the facets for both malleoli are enlarged, the crescent they form being wider; the proximal facet for the calcaneus is slightly more triangle-shaped; the medial facet is slightly wider medio-laterally; the facet for the cuboid and the distal facet for the calcaneus are anteriorly extended.

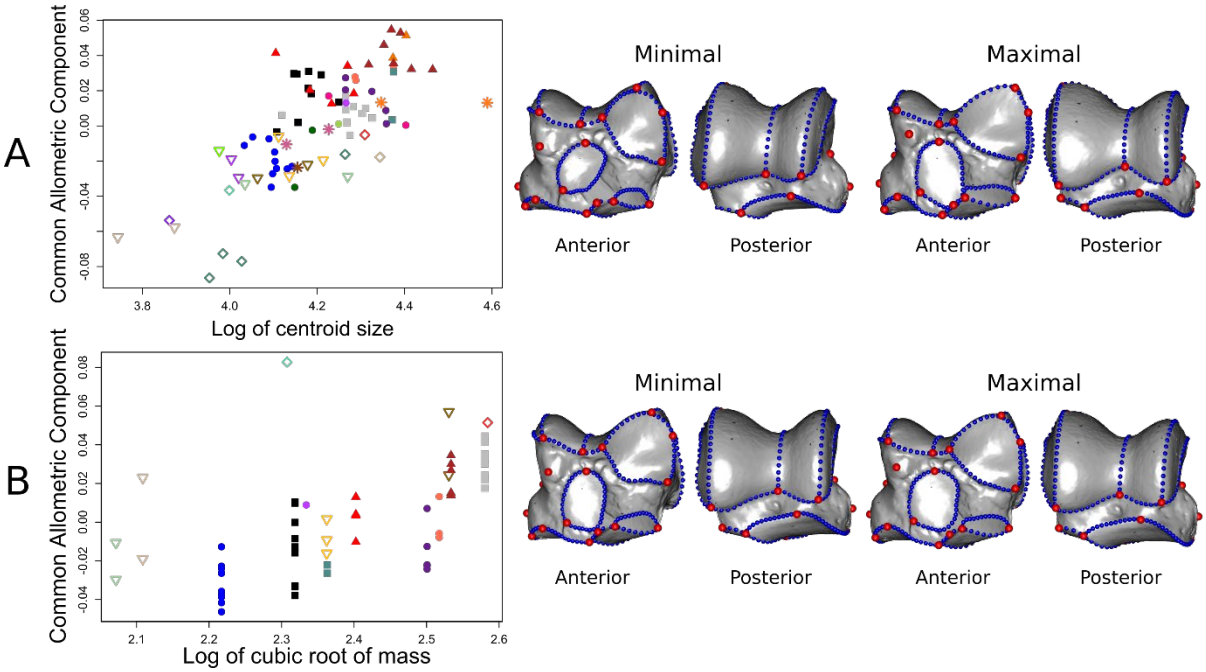

Fig. 6. A: Regression of the Common Allometric Component on the logarithm of the centroid size, with representations of the shapes corresponding to the theoretical maximum and minimum of allometry, on Rhinocerotidae astragali. B: Regression of the Common Allometric Component of allometry-free shapes, on the logarithm of the cubic root of the mean mass of the species, with representations of the shapes corresponding to the theoretical maximum and minimum of mass, on Rhinocerotidae astragali. Legend as in Fig. 5. Vector representations are available in Appendix 7B.

Calcaneus

Morphological variations

The Neighbour-Joining tree on the calcaneal morphology (Fig. 7) indicates, as for the astragalus, a tendency for individuals of the same species to be grouped together. Teleoceratina are grouped with Aceratheriina, and *Teleoceras fossiger* has again the longest branch of all species. *Elasmotherium sibiricum* has also a particularly long branch. There seem to be fewer clusters of species belonging to the same higher-rank taxon than for the astragalus. The genus *Rhinoceros*, notably, sees its three species scattered. *Ceratotherium neumayri* is close to *Chilotherium* or *Elasmotherium sibiricum*, and most of extinct dicerorhinins are grouped with *Rhinoceros palaeindicus*, *Hispanotherium beonense* and *Plesiaceratherium*. Again, for taxa of higher rank than tribes, there are not clusters following the phylogeny.

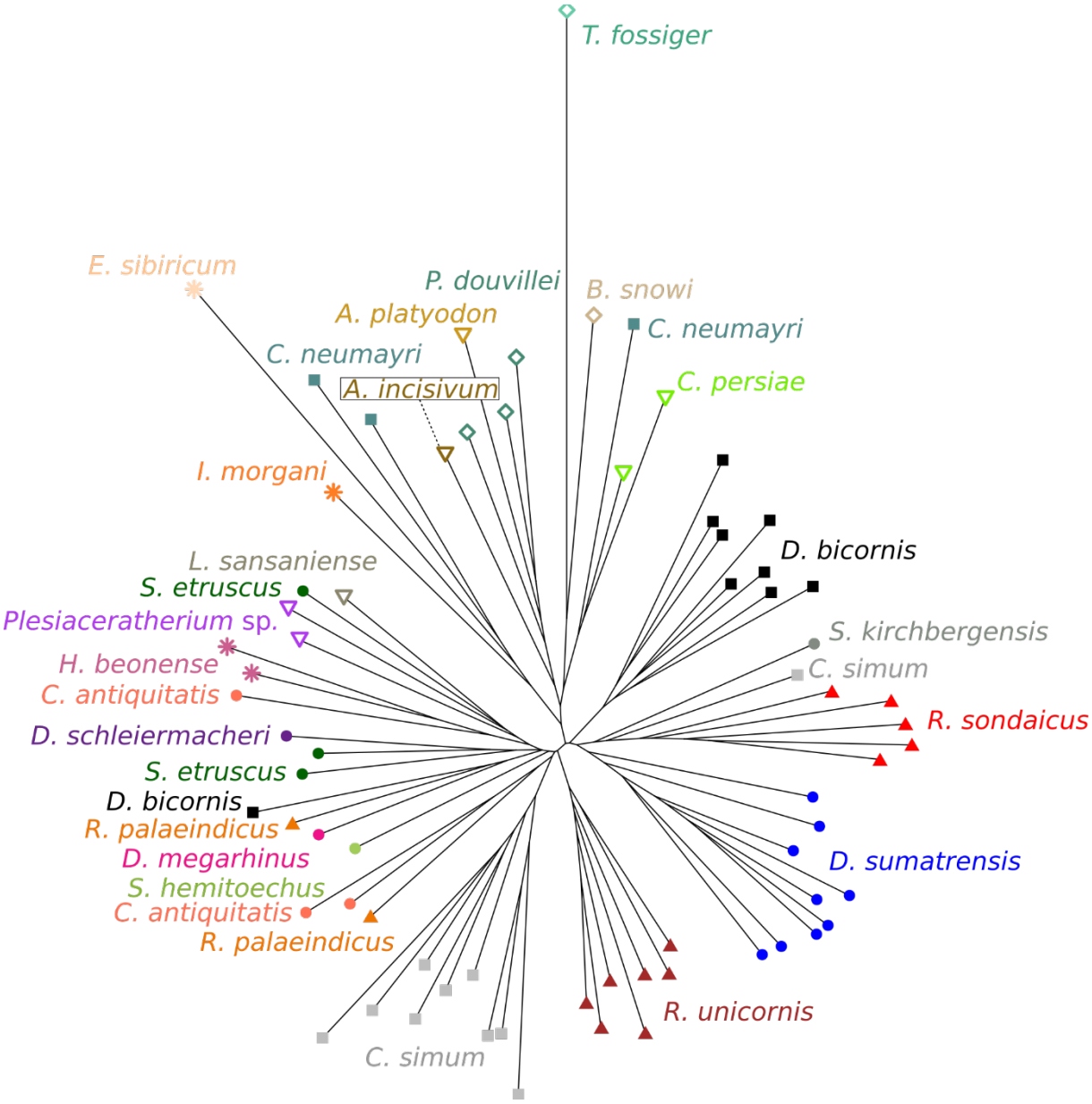

Fig. 7. Neighbour-Joining tree generated from a matrix of the Euclidian distance between every specimen, on the calcanei of Rhinocerotidae. Legend as in Fig. 8.

As for the astragalus, a low percentage of variance is explained by each axis (66.3% for the first ten axes). Only the first two axes are described, as the first one is linked to the centroid size and the second one to variations in the rhinoceroses' body plan. PC1 is weakly correlated with centroid size, negatively ($p < 0.01$, $R^2 = 0.11$).

PC1 (12.4% of variance, Fig. 8) shows *Elasmotherium* as the genus with the most negative value, along with *Ceratotherium*, *Iranotherium* and *Lartetotherium*. *Diceros* has slightly negative values, *Rhinoceros* slightly positive values. *Dicerorhinus*, *Teleoceras* and *Brachypotherium* have the most positive values on this axis. The axis is characterized in its negative extremity by a more robust tuber calcanei; a proximal facet for the astragalus that is

medio-laterally wider in its proximal half, and distally extended; a longer distal facet for the astragalus; and a larger, proximally extended facet for the cuboid whereas it is piriform (proximally reduced and distally extended) on the positive part of the axis.

PC2 (11.1%, Fig. 8) separates strongly our *Teleoceras* specimen on the negative part from the other genera. The other Teleoceratina, *Chilotherium* and *Aceratherium*, have, among the other genera, the most positive values and thus are the closest to *Teleoceras*. PC2 is characterized in its positive extremity by a more gracile tuber calcanei; a reduction of the medio-lateral width of the proximal part of the proximal facet for the astragalus; a medio-laterally wider and distally longer distal part of the proximal facet for the astragalus than on the negative extremity of the axis; a proximo-distally compressed medial facet for the astragalus, twice as wide as it is high; a much less elongated distal facet for the astragalus; and an antero-posteriorly compressed facet for the cuboid.

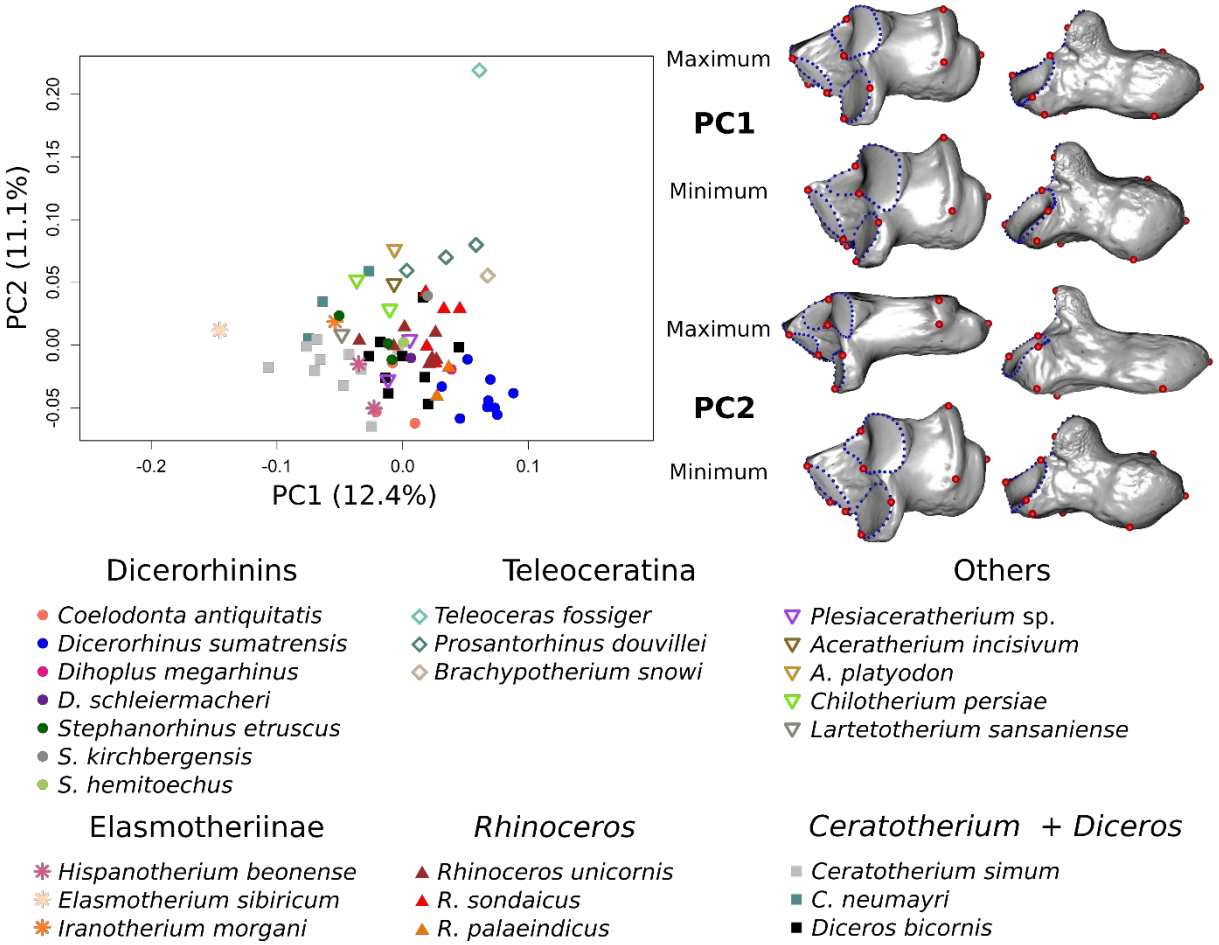

Fig. 8. Results of the PCA performed on the calcanei of Rhinocerotidae. Left: repartition of the Rhinocerotidae calcanei studied across the first two PCA axes. Right: TPS deformation of a mean shape towards the maximal and minimal values of each axis. The view is first antero-medial then postero-medial. Red dots denote landmarks, blue dots denote curve semi-landmarks. Vector representations of the deformations are provided in Appendix 7C.

Impact of allometry and mass

The centroid size has a significant but weak effect on the calcaneus shape ($p < 0.01$ and $R^2 = 0.04$; multivariate regression). A large calcaneus (Fig. 9A) has a medio-laterally wider proximal part of the proximal facet for the astragalus; a wider medial facet for the astragalus, expanding distally and merging with the distal facet for the astragalus; an elongated distal facet for the astragalus; and a sustentaculum tali oriented more distally, whereas it is oriented antero-distally in small calcanei.

The mass has a slightly stronger influence on the allometry-free shapes of the calcaneus than on those of the astragalus ($p < 0.001$, $R^2 = 0.06$). A calcaneus belonging to a heavy species (Fig. 9B) has a more robust tuber calcanei than a calcaneus belonging to a light species; the proximal facet for the astragalus is more triangular, and slightly extended medially; the distal facet for the astragalus is extended distally; and the facet for the cuboid is piriform, and wider proximally.

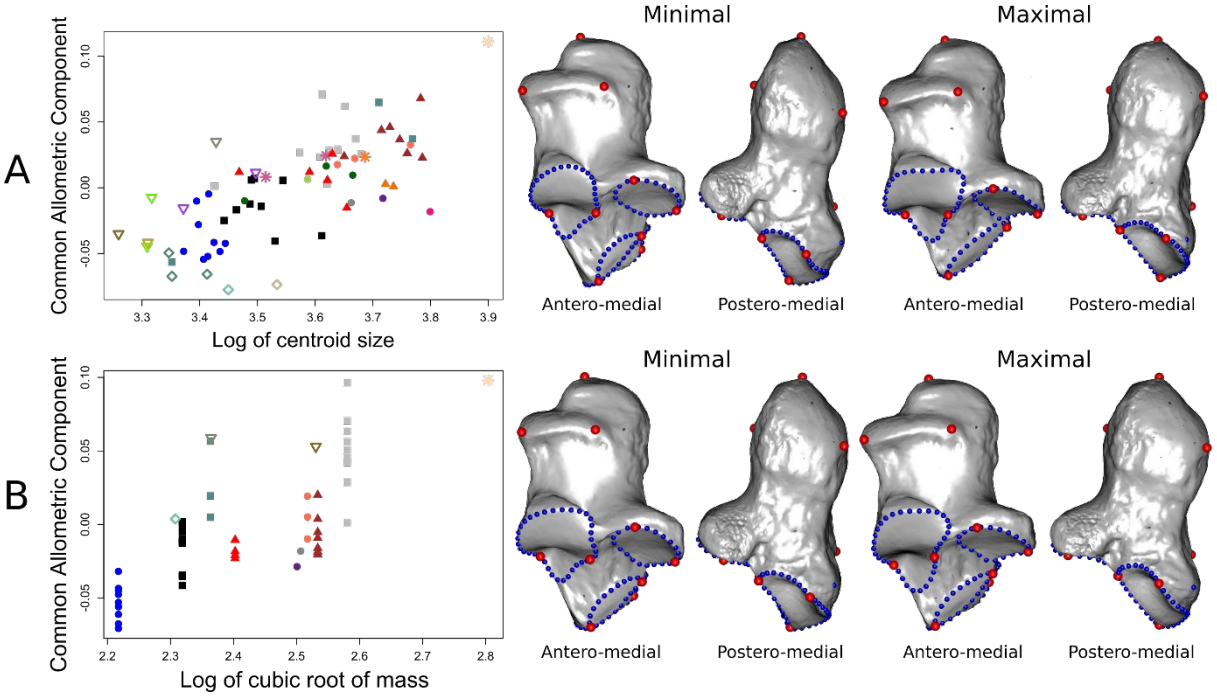

Fig. 9. A: Regression of the Common Allometric Component on the logarithm of the centroid size, with representations of the shapes corresponding to the theoretical maximum and minimum of allometry, on Rhinocerotidae calcanei. B: Regression of the Common Allometric Component of allometry-free shapes, on the logarithm of the cubic root of the mean mass of the species, with representations of the shapes corresponding to the theoretical maximum and minimum of mass, on Rhinocerotidae calcanei. Legend as in Fig. 8. Vector representations are available in Appendix 7D.

Perissodactyla

Astragalus

The Neighbour-Joining tree on the astragalar morphology (Fig. 10) shows a relative clustering of the families. However, there are exceptions. *Moropus* is not grouped with the other chalicotheres but is closer in morphology to the Rhinocerotidae, although it has a long branch, which indicates a particular morphology. *Kalobatippus*, a three-toed anchitheriine equid from the Oligocene, has a morphology closer to tapirs and rhinocerotids than to a modern one-toed equinine or hipparionine equid. The Teleoceratina are found relatively close to *Paraceratherium*, and to a lesser extent to the Chalicotheriinae, as compared to other rhinocerotids. *Teleoceras* itself is the closest to the Chalicotheriinae, sharing with them an extremely proximo-distally flattened astragalus. Families are not grouped together according to phylogenetic proximity.

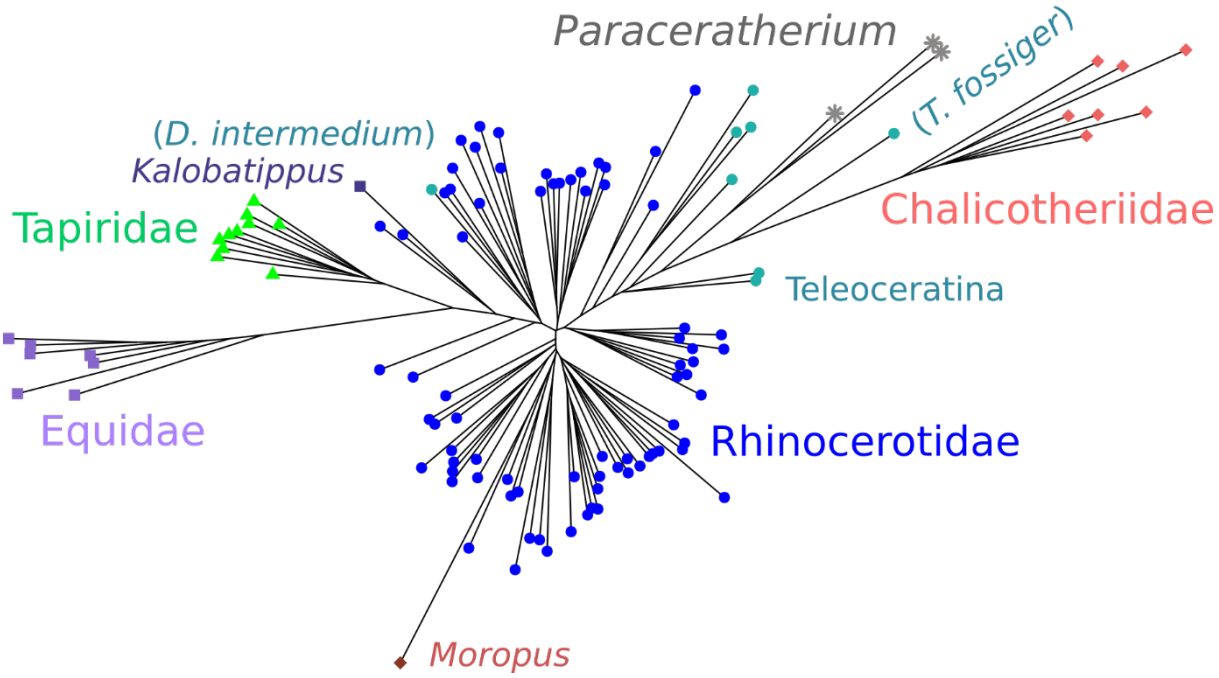

Fig. 10. Neighbour-Joining tree generated from a matrix of the Euclidian distance between every specimen, on the astragali of Perissodactyla. Extant species are represented as dots and extinct species, as squares. Teleoceratina, *Kalobatippus* and *Moropus* belong to Rhinocerotidae, Equidae and Chalicotheriidae, respectively, but are highlighted with regard to their particular positions in the tree. Legend as in Fig. 11.

The first three axes of the PCA are presented, as only those axes describe clear shape variations between the families studied, and are correlated with the centroid size (PC1 and PC3, negatively: $p < 0.0001$, $R^2 = 0.28$ and $p < 0.001$, $R^2 = 0.19$ respectively; PC2, positively: $p < 0.01$, $R^2 = 0.05$). PC1 and PC3 are more strongly correlated with centroid size than on the

analysis with only the Rhinocerotidae, but the R-square remains well below 50%. The first ten axes explain 77.8% of variance.

PC1 (37.2% of variance, Fig. 11) separates five different groups: on the most positive part of the axis are the Equinae. Less positive are the Tapiridae, plus *Kalobatippus*. Around 0 are the Rhinocerotidae, except the Teleoceratina, plus *Moropus*. On the negative side are first *Paraceratherium* and the Teleoceratina, our *Teleoceras* specimen having the most negative value of them. With the most negative values are the Chalicotheriinae, the chalicotheres with very short hindlimbs. PC1 is characterized in its negative extremity by a great proximo-distal compression of the bone, twice as wide medio-laterally as high proximo-distally, whereas astragali on the positive end of the axis are approximately equal in width and height. The negative extremity of the axis is also characterized by a very flat trochlea with medio-laterally wide, low ridges and a shallow groove, oriented proximally whereas the trochlea has very high ridges, a very deep groove and is oriented anteriorly on the positive end of the axis; and an extended facet for the fibular malleolus, occupying almost all of the lateral face of the astragalus. Finally, the negative part of PC1 presents a triangular and flat proximal facet for the calcaneus, whereas it is more squared and concave, with a latero-distal extension, on the positive side; a round medial facet for the calcaneus, whereas it is proximo-distally elongated on the positive end of the axis; and an overall wider and flatter facet for the navicular, positioned directly below the body of the astragalus.

PC2 (12.4 % of variance, Fig. 11) separates Equidae (except *Kalobatippus*) and Chalicotheriidae (except *Moropus*) on the negative side from the other families which have more positive values, *Paraceratherium* having the most positive values among them. Astragalar shape variations along PC2 are characterized in the negative extremity by the symmetry of the trochlea, each ridge being of similar height and width whereas the lateral ridge is relatively much wider on the positive end of the axis; the deeper groove of the trochlea; and the greater angular extent of the trochlea. The negative part of PC2 is also characterized by the round shape of the proximal facet for the calcaneus, with a latero-distal extension, whereas it is more square-shaped on the positive end of the axis; the wider medial facet for the calcaneus, positioned very distally, on the edge of the posterior face; the concavity of the lateral contour of the facet for the navicular; the great flatness of the facet for the navicular, whereas it is antero-posteriorly convex on the positive end of the axis; and its position medially offset from the centre of the bone.

On PC3 (8.6% of variance, Fig. 11) are spread, roughly, from negative values to positive values, *Paraceratherium*, the Rhinocerotidae and the Equidae, the Chalicotheriidae, and the

Tapiridae, although there is generally an overlap between groups. It is characterized at its negative extremity by a slightly less symmetrical trochlea, with a wider and lower lateral ridge; a distally extended lateral ridge of the trochlea; a smaller facet for the fibular malleolus, occupying a smaller part of the lateral face of the bone than it does on the positive end of the axis. The negative section of PC3 morphospace is also characterised by a latero-distally extended proximal facet, and a smaller medial facet for the calcaneus which is positioned more proximally. By comparison, bones in the positive end of PC3 possess medial facets which border the distal side of the posterior face.

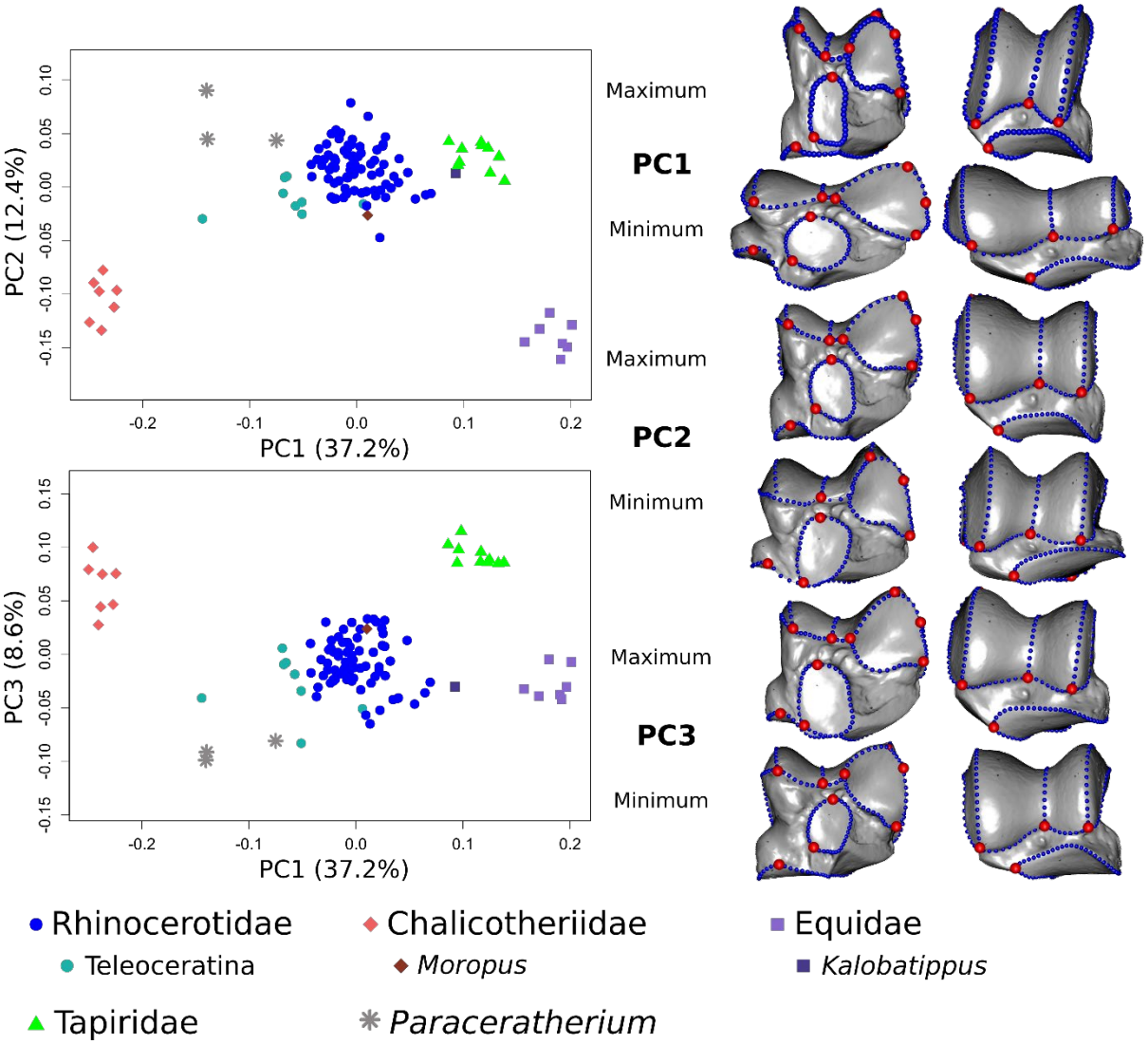

Fig. 11. Results of the PCA performed on the astragalus of Perissodactyla. Left: repartition of the Perissodactyla astragali studied across the first three PCA axes. Right: TPS deformation of a mean shape towards the maximal and minimal value of each axis. The view is first posterior then anterior. Red dots denote landmarks, blue dots denote curve semi-landmarks. Vector representations of the deformations are provided in Appendix 7E.

Impact of allometry and mass

The centroid size of the astragalus has a significant effect on its shape ($p < 0.001$ and $R^2 = 0.14$ for the astragalus, multivariate regression). A large-sized astragalus (Fig. 12A) is characterized by an overall flat bone, twice as wide medio-laterally as high proximo-distally; medio-laterally wide and low trochlear ridges; a trochlea oriented proximally; a medio-laterally wide and triangle-shaped proximal facet for the calcaneus; a round-shaped medial facet for the calcaneus; a wide facet for the navicular, flat overall and positioned below the body of the astragalus. A small sized astragalus is as wide as it is high, has higher trochlear ridges and a deeper trochlear groove; a more square-shaped proximal facet for the calcaneus, with a small latero-distal extension; a rectangle-shaped medial facet for the calcaneus, higher proximo-distally than wide medio-laterally; and a smaller facet for the navicular, not directly below the body of the astragalus but medially offset.

Species mass has a statistically significant but very weak effect on allometry-free astragalus shape ($p < 0.05$, $R^2 = 0.027$). An astragalus pertaining to a heavier species (Fig. 12B) has a flatter trochlea with lower ridges; a triangle-shaped proximal facet for the calcaneus; and a medial facet for the calcaneus located more laterally.

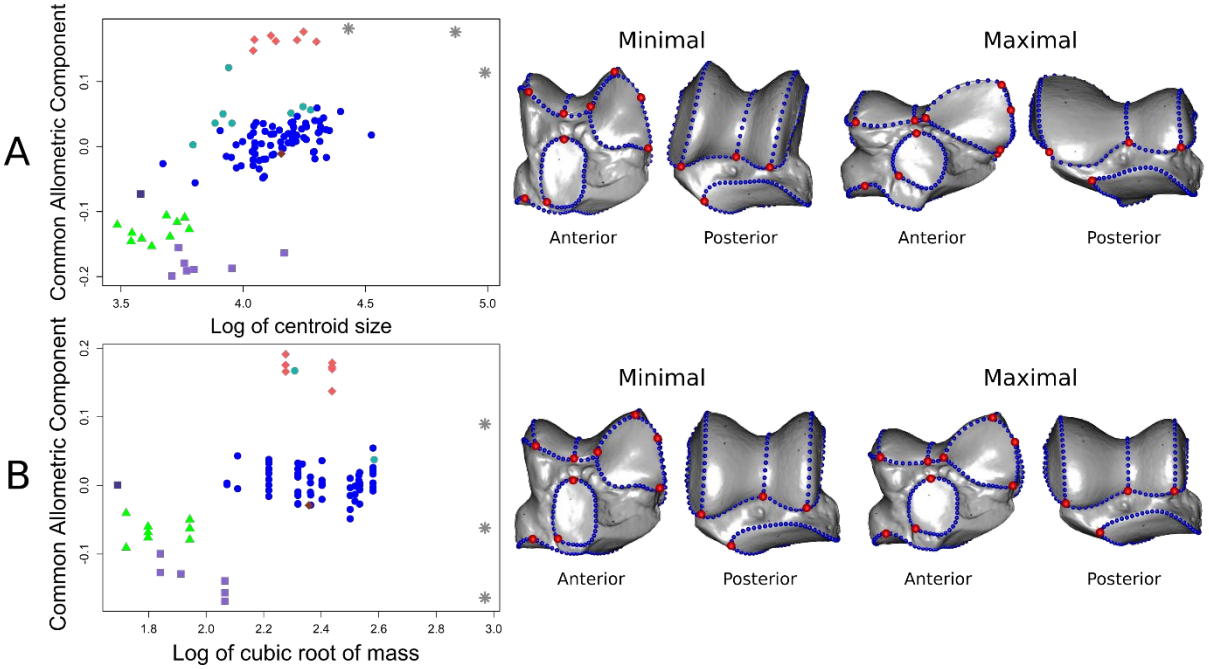

Fig. 12. A: Regression of the Common Allometric Component on the logarithm of the centroid size, with representations of the shapes corresponding to the theoretical maximum and minimum of allometry, on Perissodactyla astragali. B: Regression of the Common Allometric Component of allometry-free shapes, on the logarithm of the cubic root of the mean mass of the species, with representations of the shapes corresponding to the theoretical maximum and

minimum of mass, on Perissodactyla astragali. Legend as in Fig. 11. Vector representations are available in Appendix 7F.

Calcaneus

The Neighbour-Joining tree on the calcaneus morphology (Fig. 13) also shows a relative homogeneity of the families. The closest specimen to the *Paraceratherium* specimen is *Teleoceras fossiger*. Contrary to what was observed on the astragalus, *Moropus* is grouped with the others Chalicotheriidae, although it is not as close to them as they are to each other. Again, families are not grouped following their phylogenetic relationships.

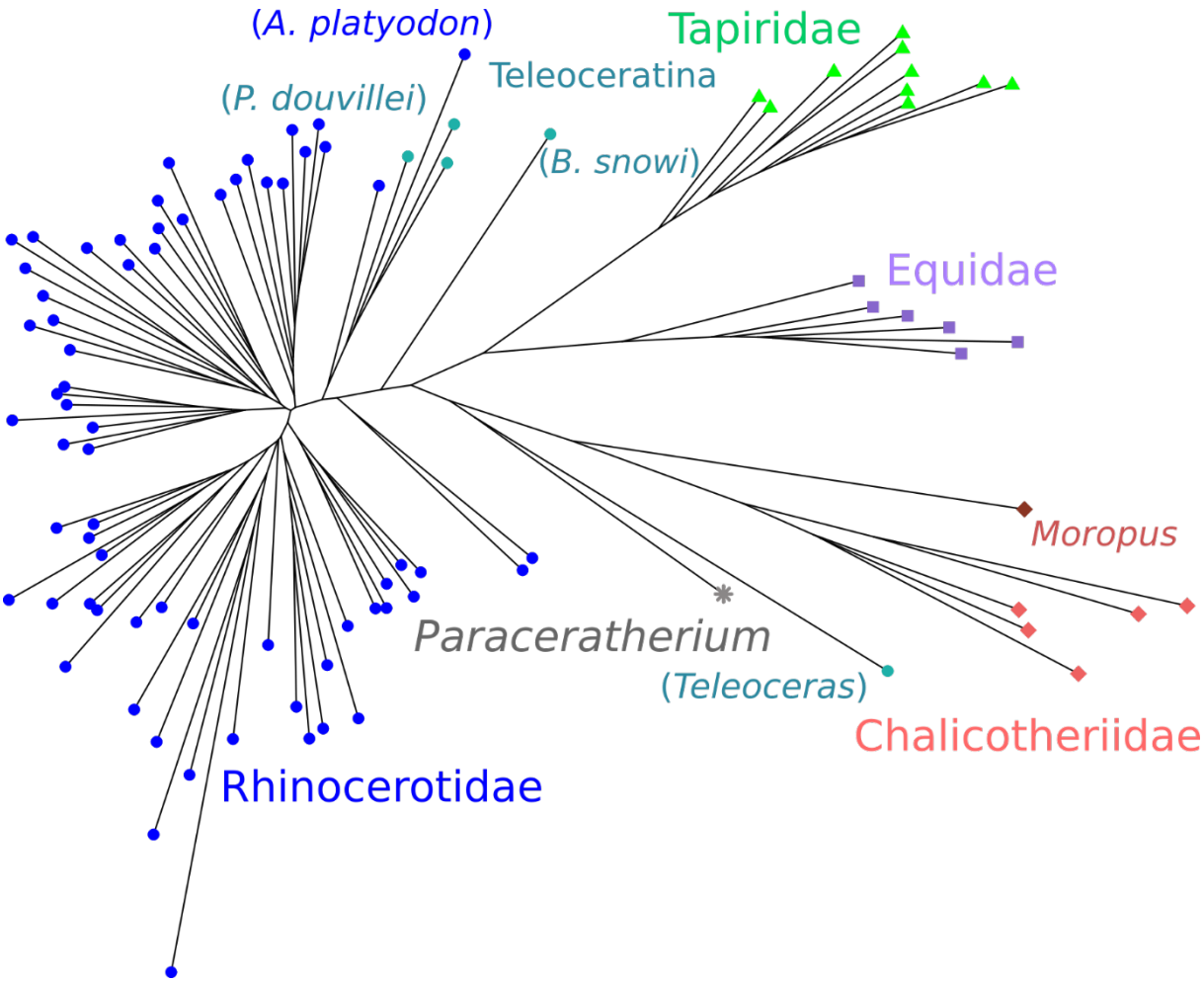

Fig. 13. Neighbour-Joining tree generated from a matrix of the Euclidian distance between every specimen, on the calcanei of Perissodactyla. Teleoceratina and *Moropus* belong to Rhinocerotidae and Chalicotheriidae, respectively, but are highlighted with regard to their particular positions in the tree. Legend as in Fig. 14.

The first two axes are described, as both of them are correlated to the centroid size and show clear distinctions between families. PC1 and PC2 are positively correlated with centroid size ($p < 0.001$, $R^2 = 0.27$ and $p < 0.01$, $R^2 = 0.08$, respectively). Again, PC1 is more strongly correlated

in size than on the analysis with Rhinocerotidae alone, but the R-square remains well below 0.5. The first ten axes explain 79.3% of variance.

PC1 (31% of variance, Fig. 14) separates (from the most negative values to the most positive values): the Tapiridae, the Equidae, the Chalicotheriidae, and the Rhinocerotidae along with *Paraceratherium*. It is characterized in its negative extremity by a much more elongate and thin tuber calcanei; a relatively smaller proximal facet for the astragalus, reduced proximally, distally and anteriorly; and a smaller facet for the cuboid, narrower because of a postero-lateral reduction.

PC2 (16% of variance, Fig. 14) strongly separates the Chalicotheriidae on the positive side from all the others. Our specimen of *Moropus* has a slightly less positive value than the Chalicotheriinae, and the Tapiridae have more negative values than the Equidae, Rhinocerotidae and *Paraceratherium*. The axis is characterized in its positive extremity by a more elongate and thin tuber calcanei; a head of the calcaneus that is much shorter, accounting for approximately one third of the total length of the bone whereas on the negative end, it accounts approximately for one half; a slightly wider, more distally oriented and much more proximally-positioned facet for the cuboid, almost in contact with the proximal facet for the astragalus; a proximal facet for the astragalus distally very extended; and a wider medial facet for the astragalus, extended medially.

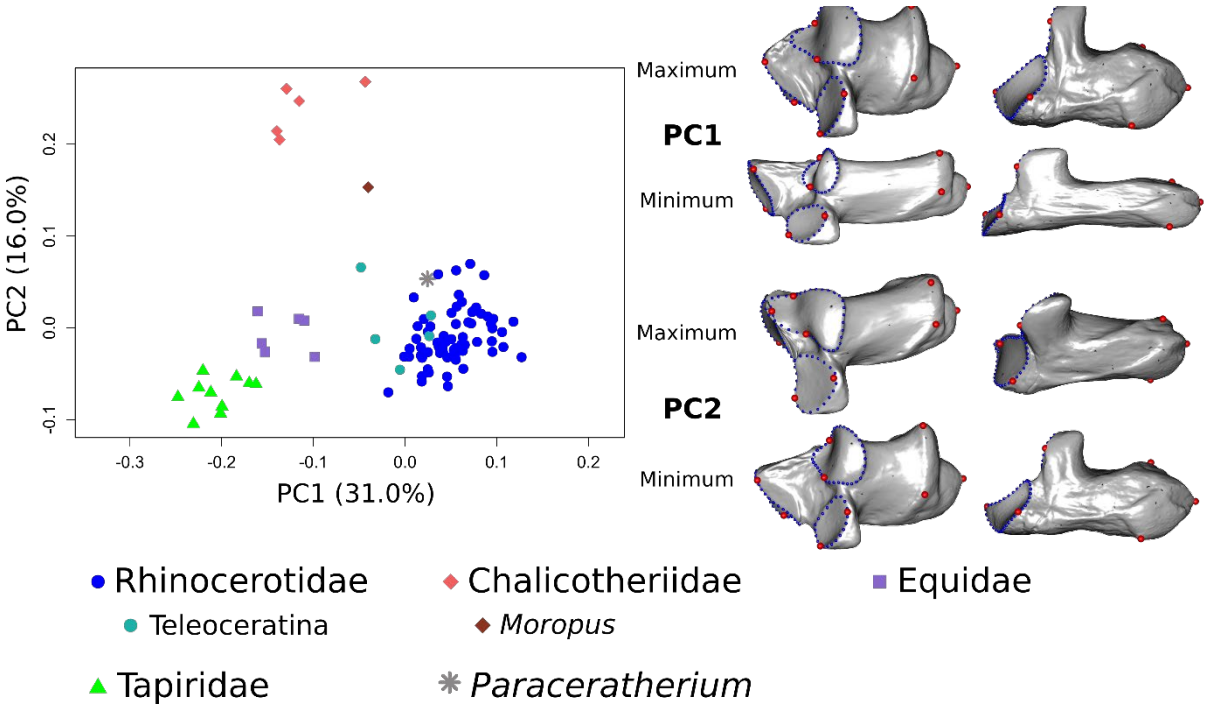

Fig. 14. Results of the PCA performed on the calcaneus of Perissodactyla. Left: repartition of the Perissodactyla calcanei studied across the first two PCA axes. Right: TPS deformation of a mean shape towards the maximal and minimal value of each axis. The view is first antero-

medial then postero-medial. Red dots denote landmarks, blue dots denote curve semi-landmarks. Vector representations of the deformations are provided in Appendix 7G.

Impact of allometry and mass

The centroid size of the calcaneus has a significant influence on its shape ($p < 0.001$ and $R^2 = 0.11$, multivariate regression). A large-sized calcaneus (Fig. 15A) is characterized by an extreme proximo-distal compression, the tuber calcanei being very robust; a much wider proximal facet for the astragalus, extended in all directions, especially in its proximal half; a distally-oriented sustentaculum tali and medial facet for the astragalus; and a wider facet for the cuboid, triangle-shaped and latero-posteriorly extended. A small-sized calcaneus has a very thin tuber calcanei as compared to large-sized ones; a relatively much smaller overall proximal facet for the astragalus; an anteriorly oriented sustentaculum tali and medial facet for the astragalus; and a relatively smaller facet for the cuboid.

There is a statistically significant influence of species mass on allometry-free calcaneus shape ($p < 0.001$, $R^2 = 0.09$). Shape differences are clear (Fig. 15B), unlike those observed for that same analysis on Rhinocerotidae alone. In our sample, a calcaneus belonging to a heavier species is, on average, characterized by a stouter tuber calcanei; a wider overall proximal facet for the astragalus; a slightly wider medial facet for the astragalus, oriented distally along with the whole sustentaculum tali; and a wider facet for the cuboid, expanding more proximally.

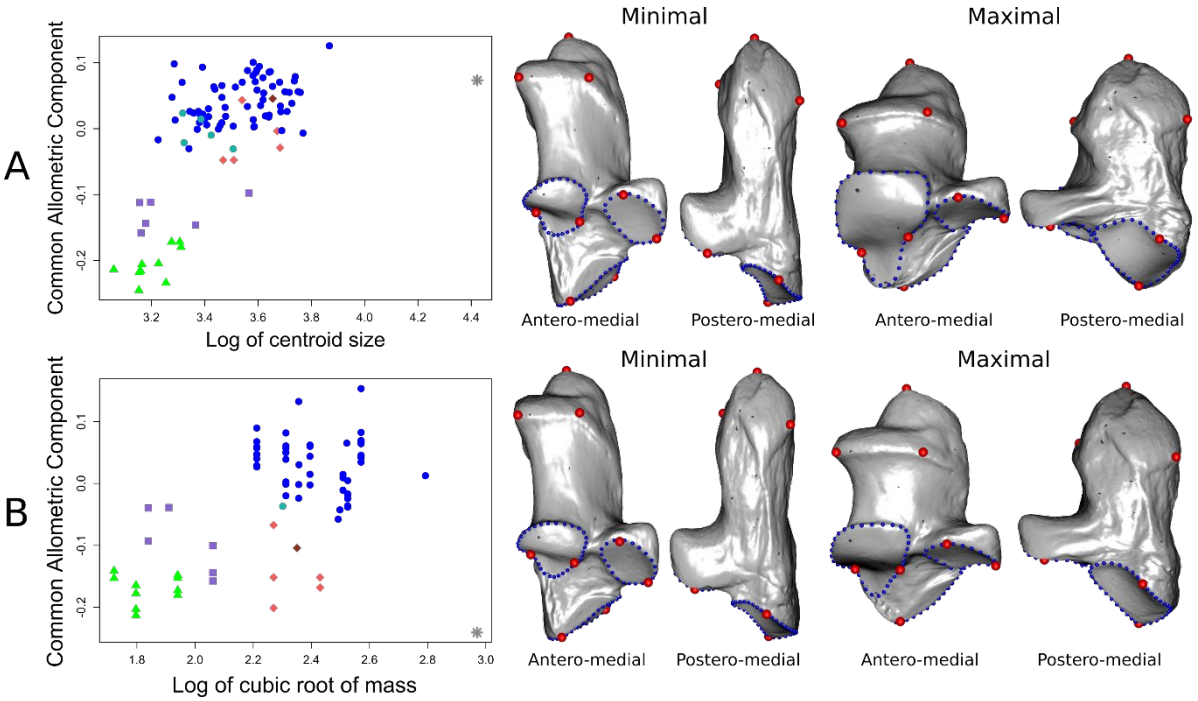

Fig. 15. A: Regression of the Common Allometric Component on the logarithm of the centroid size, with representations of the shape corresponding to the theoretical maximum and minimum

of allometry, on Perissodactyla calcanei. B: Regression of the Common Allometric Component of allometry-free shapes, on the logarithm of the cubic root of the mean mass of the species, with representations of the shape corresponding to the theoretical maximum and minimum of mass, on Perissodactyla calcanei. Legend as in Fig. 14. Vector representations are available in Appendix 7H.

Discussion

First and foremost, it is worth noting that the percentage of variance explained by the first axes of the PCA is usually low (around 66% for the first five axes for the Perissodactyla dataset, 40% for the Rhinocerotidae dataset). The first four or five axes describe the variations between species or families, but the following axes usually distinguish one or two individuals from other specimens of the same taxon. There is indeed a great intraspecific variation in the species studied, even if it remains inferior to inter specific variations (Figs. 4, 7). For example, *Dicerorhinus sumatrensis* ZSM-1908-571 presents an astragalus with a wide medio-distal extension of the medial facet for the calcaneus, an extension absent in all the other specimens. Some specimens of *Ceratotherium simum* present a calcaneus with a fusion of the medial and distal facets for the astragalus, whereas in others they are separated by a deep groove. This could explain the low PC-score values. Indeed, if there are many different variations observed in the sample, these cannot be described on one PC alone and thus the percentage of variation explained by the first axes lowers. On the other hand, if there were a factor clearly driving a continuum of variations in all our sample, we would see a higher percentage of variance for the first axis. That factor is often size (see e.g. Bonnan *et al*., 2013; Cardini *et al*., 2015; Knigge *et al*., 2015); here it seems clear that size does not have a strong influence on the shape of the bones, especially in our Rhinocerotidae dataset. We already noted qualitatively this intraspecific variability between individuals of the same species of Rhinocerotidae when digitizing the bones, and it has also been observed by Guérin (1980) on various bones of the tarsus of extant rhinocerotids, by Harrison & Manning (1983) on the carpus bones of *Teleoceras*, and by Heissig (2012) on several limb bones, including the astragalus, of aceratheres. Variations in the age of the specimens, especially for individuals for which we have only an astragalus and no calcaneus or long bones associated, could account for some intraspecific variation. It is difficult to determine the age of individuals using only the astragalus, considering there are no epiphysis on this bone. Additionally, the high number of species, mostly with only one or two individuals, could also result in a greater diversity of morphological variations in our sample and thus lower the variance explained by the first axes. Finally, it seems that Rhinocerotids are a relatively conserved group in terms of the morphology of their astragalus and calcaneus. This could mean that PC scores are more driven by small, individual-specific or species-specific variations than by large-scale variations such as variations linked to size or mass.

General influence of mass

The centroid size of both the astragalus and calcaneus has an effect on their shape (Figs. 6, 9). Considering that the centroid size of the bone is linked to the mean mass of the species it belongs to (Appendix 5), especially on the Perissodactyla dataset, this means that mass has an influence on the shape of the bones in our sample of Perissodactyla. The percentage of variance explained by the centroid size or the mass, however, is lower than we originally expected. We could indeed expect mass to have a very strong influence on the shape of limb bones, explaining at least 50% of the total variance (Hildebrand *et al.*, 1985; Biewener, 1989; Campione & Evans, 2012). It seems that, especially when studying only rhinocerotids' astragali and calcanei, which do not vary much in terms of shape, size has no overwhelming influence on the shape of the bone but is instead one factor among others (e.g. possibly habitat, phylogeny and intraspecific variations). Another study on the limb long bones of extant rhinocerotids found a relatively low influence of centroid size on the shape of the bones, although higher than what is observed here (R-square between 10 and 18%; Mallet *et al*., 2019). It is therefore possible that long bones are more affected by size than astragalus and calcaneus.

When centroid size increases, both the astragalus and the calcaneus present an increase in the size of the articular facets. Moreover, in the analysis on Rhinocerotidae alone, the distal and medial facets of each bone for the articulation with the other are fused in specimens with a high centroid size. It could be suggested that wider facets result in a more intricate association between the bones, making the talocalcaneal complex more suited to dissipate compressive forces during limb loading, during plantarflexion or dorsiflexion of the foot (i.e. flexion or extension of the ankle). In the large astragali belonging to Perissodactyla, the trochlea is oriented proximally, directly facing the tibia and fibula, and has a lower angular extent (Fig. 12). One can assume that this orientation permits a complete unfolding of the crurotarsal joint, putting the foot in the exact same axis as the rest of the limb. This results in a general columnar posture for the limb, as is characteristic of graviportal animals. This columnar posture would help resist twisting, bending and compression forces, and reduce the possibility of dorsiflexion of the autopodium, reducing running speed (Hildebrand, 1982). It has already been said that *Paraceratherium* had columnar limbs (Osborn, 1923; Prothero, 2013), and our results corroborate that statement, for the hind autopodium-zeugopodium at least. It can be assumed that the flatter trochlea observed in large astragali, associated with a proximal-distal compression of the bone, fulfils the same role of resistance to twisting and compression. A deeper trochlea would provide more stability for the crurotarsal joint (Polly, 2008), but lead to

thinner and therefore more fragile ridges of the trochlea, unable to resist the high forces expected on the ankle of a very heavy animal. This flattening is also observed in Brontotheriidae (Osborn, 1929), Elephantidae (Csuti *et al.*, 2008), and sauropod dinosaurs (Bonnan, 2005), which supports our hypothesis.

For large-sized calcanei belonging to Perissodactyla, beyond the increasing size of the articular surfaces, the main characteristic is that the tuber calcanei is more robust, thicker both medio-laterally and antero-posteriorly, and shorter proximo-distally compared to the total length of the calcaneus (Fig. 15). However, this is only clearly observable when studying our Perissodactyla dataset. The tuber calcanei is a lever arm for the plantarflexion of the foot; with two of the muscles inserting on it being responsible for plantarflexion: the gastrocnemius and the soleus (Beddard & Treves, 1889; White & Folkens, 2005). A more robust and shorter tuber would presumably lead to a lower mechanical advantage, requiring a weaker pull from the muscles, which would be easier to resist and reduce bending stress. It could also be a consequence of the proximo-distal shortening of the foot generally observed in heavier species of our sample (Rhinocerotidae, Chalicotheriidae).An animal with an elongated foot would need a longer tuber calcaneus to keep the mechanical advantage constant; conversely, an animal with a short foot would not need a very long lever arm, presuming the mechanical advantage is indeed constant (Biewener, 1989). The correlation of the mean mass of the species on allometry-free shapes of the calcaneus corroborates this result. For two calcanei of the same size but belonging to species of different masses, the one belonging to the heaviest species will have a more robust tuber and wider articular facets (Fig. 15B). This is observable in our analysis in *C. simum* and *R. unicornis*: *C. simum* is heavier and has a slightly more robust calcaneus, but on average, the centroid size of its calcaneus is smaller than that of *R. unicornis* (Figs. 5, 6). This increased robustness of the body of the calcaneus is found in other mammal families of high body mass (i.e. more than about two tons), such as Elephantidae (Chen & Tong, 2017), and also in fossils such as *Pyrotherium* (Shockey & Anaya Daza, 2004). Interestingly, this is not the case in Hippopotamidae which have a rather elongate calcaneus (see e.g. Fig. 6 and 8 in Fisher *et al.* [2010]). Hippopotamuses have a body plan close to Teleoceratina, with very short limbs, which also present an elongate calcaneus. Possibly the forces exerted on the calcaneus are less intense for animals with short legs; comparisons with e.g. Suidae and Amynodontidae could yield insights in this regard.

Particular cases linked to body plan and locomotion

As expected, some observed variations in bone shape appear to be linked to the diverse body plans and modes of locomotion of the taxa studied. For the astragalus, equids are characterized by the great depth of their trochlea, a common characteristic in cursorial mammals allowing a stabilization of the crurotarsal joint by restricting movement to a parasagittal plan (Polly, 2008). The trochlea is also moderately deep in Rhinocerotidae (except most Teleoceratina) and Tapiridae, but not in our Chalicotheriinae, animals that most likely could not gallop (Coombs, 1983). Teleoceratina specimens also possess very shallow trochleas. Considering their similarity in terms of body-plan with hippopotamuses, which cannot gallop (Lewison 2011), it is likely that they could not gallop either, and the shape of their astragalus is consistent with this. *Paraceratherium* and the Chalicotheriinae possess the flattest trochlea of all of our specimens, but still with clearly distinguishable ridges (Figs. 11, 12), unlike elephants for instance (see e.g. Scarborough *et al*., 2016). Equids also display a greater angular extent of their trochlea, presumably allowing a greater flexion and extension of the ankle. The most cursorial species (i.e. equids and, to a lower extent, tapirs) possess, on their astragalus, curved facets for the navicular and a curved proximal facet for the calcaneus, whereas those facets are mostly flat in *Paraceratherium* and *Chalicotherium* (Fig. 11). Perhaps the curved facets help to lock the talocalcaneal and talonavicular joints and provide stability for the ankle. The flat facets of heavy species could help homogeneously dissipate the forces in the foot and facilitate the formation of robust ridges.

A particular shape variation linked to body proportions is the proximo-distal compression of the astragalus across most of our Teleoceratina (Fig. 5). *Diaceratherium* is the only Teleoceratina from our sample presenting an astragalus similar to that of other rhinocerotids in this regard. Teleoceratina had extremely short, columnar limbs, like modern hippopotamuses. This compression of the astragalus could be linked to the general shortening of the limbs, each segment being proximo-distally shortened, including the basipodium. Interestingly, the astragalus is not compressed in *Diaceratherium intermedium*, a Teleoceratina that is phylogenetically the sister-group to the other Teleoceratina from our sample (Figs. 1, 5). It is unclear if *D. intermedium* was short-legged like the others Teleoceratina. The species was placed in the genus *Chilotherium* for a long time, before being reassigned by Antoine *et al.* in press. *Chilotherium* is characterized by short legs for its members (Geraads & Spassov, 2009), but no studies have been done specifically on *D. intermedium*. If this species was indeed short-legged, the shortening of the limbs would predate the flattening of the astragalus in our sample.

The compression of the astragalus does not seem to be dependent on the size of the animal in our Teleoceratina. This condition is observed in both small (e.g. *Prosantorhinus*; <800kg) and large (*Brachypotherium*; >2000kg) Teleoceratina (Cerdeño, 1998; Becker, 2003). It is worth noting that *Paraceratherium* presents the same flattening of the astragalus as our Teleoceratina. Both groups are indeed very close regarding the morphology of their astragalus (Figs. 10, 11). *Paraceratherium* is, however, very different from Teleoceratina in that it is very high-legged. It seems that different constraints, *i.e.* the very high mass of *Paraceratherium* and the short legs and lighter mass of Teleoceratina, can produce a similar result in terms of morphology. A study incorporating Amynodontidae (rhinocerotoids with some members, like *Metamynodon*, being short-legged like Teleoceratina, Wall, 1989), could also yield more insights on the matter. Teleoceratina astragali also differ from those of other rhinocerotids by the distal elongation of their proximal facet with the calcaneus. The facet almost reaches the distal side of the bone, whereas it reaches only halfway in other rhinocerotids (Fig. 5). The facet might need to remain relatively long in order to maintain cohesion between the astragalus and the calcaneus. Thus, when the bone is proximally reduced, the facet retains the same length and occupies relatively more space on the posterior face. *Teleoceras* being an extremely variable genus in terms of bone morphology (Harrison & Manning, 1983), a study with more individuals could yield insights on more subtle shape variations.

Chalicotheriinae also present a proximo-distally compressed astragalus. They differ from Teleoceratina and *Paraceratherium* in that their trochlea is oriented more anteriorly, and has a greater angular extent. This seems logical when looking at the angle of the crurotarsal articulation: the angle is clearly superior to 90°, almost reaching a flat angle, in *Teleoceras* and *Paraceratherium*, giving the limb a columnar posture. It is however approximatively equal to 90° in *Chalicotherium*, whose hindlimb is much more crouched (see e.g. Fig. 7B in Coombs, 1983). The extremely flattened astragalus of the Chalicotheriinae is not found in *Moropus*, which shows an astragalus closer to a rhinocerotid. The trochlea in particular is deeper in *Moropus*, whereas it is shallow in *Chalicotherium* and *Anisodon*. The extreme proximal-distal compression of Chalicotheriinae astragali could be a consequence of the reduction in the length of the hind limb, with each part of the limb being reduced, just as in Teleoceratina. This shortening could also be linked to the heavier mass carried by shorter hindlimbs, whereas body mass would be more evenly spread on fore and hindlimbs if they were of equal length. It could also be a consequence of their posture. Chalicotheriinae are indeed described as bipedal browsers. It is assumed that they could adopt an erected posture on their hindlimbs and use their

forelimbs to grasp at branches and twigs (Zapfe, 1979; Coombs, 1983; Schulz-Kornas *et al.*, 2007). Most of their weight would therefore be supported by the hindlimbs, which would be in accordance with a stronger, flatter astragalus as observed in *Paraceratherium*. *Moropus*, and presumably the Schizotheriinae in general, have hindlimbs and forelimbs of approximately the same length, and were postulated to use bipedal browsing less frequently (Coombs 1982; 1989). This would reduce the advantage of a flatter astragalus. Further studies are needed to confirm or refute these hypotheses, with more individuals belonging to more genera, especially for Schizotheriinae (e.g. *Ancylotherium* or *Metaschizotherium*).

Another bone presenting a shape much different than what would be expected if mass were the single driving factor is *Paraceratherium*'s calcaneus. *Paraceratherium* is by far the heaviest species of our sample, almost twice as heavy as *Elasmotherium* (Table 1). However, its calcaneus is elongated when compared to *Elasmotherium*'s, which has the most robust calcaneus (Figs. 15, 16). This could be a consequence of its general body plan: *Paraceratherium* had higher legs than all the rhinocerotids. One might thus suppose that longer legs, and thus, a longer autopodium like observed in *Paraceratherium* (Prothero 2013), lead to an elongation of the tuber calcanei to keep the mechanical advantage of the lever system of the foot constant. Antoine *et al.* (2004) have indeed observed similarities between the calcaneus of *Paraceratherium* and that of a *Giraffa*. However, Teleoceratina have very short legs and a rather elongated calcaneus as well compared to other rhinocerotids (Fig. 6), and elephants have high legs but a very short calcaneus. Others individuals of *Paraceratherium* and *Elasmotherium* are needed to confirm these results, as well as smaller members of the Paraceratheriidae family (e.g. *Pappaceras* and *Juxia*; Wang, 2016). A study including other families of Rhinocerotoidea, like the small cursorial Hyracondontidae and the short-legged Amynodontidae could provide a better understanding of the question. Ultimately, comparing heavy and stocky mammals, such as *Mixotoxodon* (Notoungulata, Meridiungulata) or *Hippopotamus amphibus* (Hippopotamidae), with heavy and slender mammals like *Titanotylopus* (Camelidae) or *Giraffa camelopardalis* (Giraffidae) could also help understand the adaptations in the basipodium of *Paraceratherium*. However, in these extremely disparate taxa, one must be careful for a phylogenetical signal which could mask the changes of shape linked to mass. It is unclear what gait *Paraceratherium* was capable of adopting besides walking. Paul & Christiansen (2000) have suggested it could at least attain a trot. The fact that their astragalus retains clear ridges and that their calcaneus is quite elongated, characteristics reminiscent of cursorial animals

(Polly, 2008; Bassarova *et al*., 2009), is consistent with this suggestion. Elephants possess a completely flat trochlea and a short calcaneus, and are unable of trotting or galloping.

Fig. 16. Anterior views of the calcanei of *Paraceratherium bugtiense* NHM-PAL-PV-M-100418 (Paraceratheriidae) and *Elasmotherium sibiricum* NHM-PAL-PV-M-12429 (Rhinocerotidae).

Conclusion

Overall, it seems that mass has an influence on the shape of the astragalus and calcaneus in Rhinocerotidae and in our sample of Perissodactyla. However, that influence is lower than we initially thought, especially among Rhinocerotidae alone. This seems to indicate that Rhinocerotidae is a relatively conserved group in terms of the morphology of those bones, and that other factors, such as the phylogeny or intraspecific variations, have more influence. An ecomorphological study could help determine if habitat could have a role, but would require reliable habitat assignations for the fossil species. Nonetheless, bones belonging to heavier Rhinocerotidae present larger articular facets, presumably to help better dissipate the larger forces involved in the locomotion of heavier animals. The calcaneus is also more robust. In our sample of Perissodactyla, a stronger influence of mass is noted, with again heavier facets and stronger bones overall. We observe a flattened trochlea of the astragalus that would limit the risk of breaking, as compared to lighter animals which have a deeper trochlea with thin ridges for the stability of the crurotarsal joint. Although these features can thus be explained morphofunctionally, the phylogenetic signal is significant and could also explain variations between the families. A larger study encompassing large and small species of Perissodactyla will be necessary to determine more specifically what drives the shape of these bones in this order. Moreover, comparison between rhinocerotids and other perissodactyls reveal that body plan has a clear influence on the shape of the bones. Short-legged Teleoceratina display a flattened astragalus and an elongate calcaneus. Chalicotheres with short hindlimbs also display

a flattened astragalus compared to chalicotheres with hindlimbs as long as their forelimbs, perhaps linked to the increased mass supported by the hindlimbs. Finally, *Paraceratherium*, which is extremely heavy and relatively high-legged compared to other rhinocerotoids, displays a flat astragalus as expected but a relatively elongate tuber calcanei, perhaps linked to either its elongate metapodials or to its phylogenetic history.

Acknowledgements

This work acknowledges financial support from **ERC-2016-STG GRAVIBONE** allocated to A. Houssaye. We acknowledge the very helpful comments of the three reviewers, **P.-O. Antoine** of the University of Montpellier, **J. MacLaren** of the University of Liège and **M. Mihlbachler** of the New York Institute of Technology. We wish to thank the curators of all the collections where we digitized specimens: **J. Lesur, C. Bens, A. Verguin & G. Billet** (*Muséum National d'Histoire Naturelle, Paris, France*), **E. Robert** (*Université Claude Bernard, Lyon, France*), **Y. Laurent** (*Muséum d'Histoire Naturelle de Toulouse, Toulouse, France*), **C. West, R. Jennings & M. Cobb** (*Powell-Cotton Museum, Birchington-on-Sea, United Kingdom*), **P. Brewer, R. Pappa & R. Portela Miguez** (*Natural History Museum, London, United Kingdom*), **A.H. van Heteren** (*Zoologische Staatssammlung München, Munich, Germany*), **G. Rößner** (*Bayerische Staatssammlung fur Palaöntologie und historiche Geologie, Munich, Germany*), and **F. Zachos, A. Bibl & U. Göhlich** (*Naturhistorisches Museum, Vienna, Austria*).

References

3D Systems. **2017**. *Geomagic Wrap*.

Adams DC. **2014**. A generalized K statistic for estimating phylogenetic signal from shape and other high-dimensional multivariate data. *Systematic Biology* **63**: 685–697.

Agisoft LLC. **2017**. *Agisoft PhotoScan Professional*.

Alexander R. **1985**. Body support, scaling, and allometry. In: Hildebrand M, Bramble DM, Liem KF, Wake D, eds. *Functional vertebrate morphology*. Cambridge, USA: Belknap Press of Harvard University Press, 26–37.

Antoine PO. **1997**. *Aegyrcitherium beonensis*, nouvel élasmothère (Mammalia, Perissodactyla) du gisement miocène (MN 4b) de Montréal-du-Gers (Gers, France). Position phylogénétique au sein des Elasmotheriini. *Neues Jahrbuch für Geologie und Paläontologie - Abhandlungen* **204**: 399–414.

Antoine PO. **2002**. Phylogénie et évolution des Elasmotheriina (Mammalia, Rhinocerotidae). *Mémoires du Muséum national d'Histoire naturelle* **188**: 1–359.

Antoine PO, Shah SMI, Cheema IU, Crochet JY, De Franceschi D, Marivaux L, Métais G & Welcomme JL. **2004**. New remains of the baluchithere *Paraceratherium bugtiense* (Pilgrim, 1910) from the Late/latest Oligocene of the Bugti hills, Balochistan, Pakistan. *Journal of Asian Earth Sciences* **24**: 71–77.

Antoine PO, Downing KF, Crochet JY, Duranthon F, Flynn LJ, Marivaux L, Métais G, Rajpar AR & Roohi G. **2010**. A revision of *Aceratherium blanfordi* Lydekker, 1884 (Mammalia: Rhinocerotidae) from the Early Miocene of Pakistan: postcranials as a key. *Zoological Journal of the Linnean Society* **160**: 139–194.

Antoine, PO. In press. Rhinocerotids from the Siwalik faunal sequence. In: Badgley, C, Pilbeam, D & Morgan, M, eds., *At the foot of the Himalayas: paleontology and ecosystem dynamics of the Siwalik record of Pakistan.* Johns Hopkins University Press.

Artec 3D. **2018**. *Artec Studio Professional*.

Barr WA. **2014**. Functional morphology of the bovid astragalus in relation to habitat: controlling phylogenetic signal in ecomorphology. *Journal of Morphology* **275**: 1201–1216.

Bassarova M, Janis CM & Archer M. **2009**. The calcaneum—on the heels of marsupial locomotion. *Journal of Mammalian Evolution* **16**: 1–23.

Becker D. **2003**. *Paléoécologie et paléoclimats de la Molasse du Jura (Oligo-Miocène) : apport des Rhinocerotoidea (Mammalia) et des minéraux argileux*. Doctoral dissertation, Université de Fribourg.

Beddard FE & Treves F. **1889**. On the anatomy of *Rhinoceros sumatrensis*. *Proceedings of the Zoological Society of London* **57**: 7–25.

Biewener A. **1989**. Mammalian terrestrial locomotion and size. *BioScience* **39**: 776–783.

Biewener A. **1990**. Biomechanics of mammalian terrestrial locomotion. *Science* **250**: 1097–1103.

Biewener A & Patek S. **2018**. Physical and Biological Properties and Principles. In: *Animal Locomotion*. New York: Oxford University Press, 1-11

Blomberg SP, Garland T & Ives AR. **2003**. Testing for phylogenetic signal in comparative data: behavioral traits are more labile. *Evolution; International Journal of Organic Evolution* **57**: 717–745.

Bongianni M. **1988**. *Simon & Schuster's guide to horses and ponies*. New York: Fireside.

Bonnan MF. **2005**. Pes anatomy in sauropod dinosaurs: implications for functional morphology, evolution, and phylogeny. In: Tidwell, V & Carpenter, K. eds., *Thunder-lizards: the sauropodomorph dinosaurs*. Bloomington: Indiana University Press, 346–380.
Bonnan MF, Wilhite DR, Masters SL, Yates AM, Gardner CK & Aguiar A. **2013**. What lies beneath: sub-articular long bone shape scaling in eutherian mammals and saurischian dinosaurs suggests different locomotor adaptations for gigantism. *PLoS ONE* **8(10)**: e75216.
Bookstein FL. **1991**. *Morphometric tools for landmark data: geometry and biology*. Cambridge: Cambridge University Press.
Botton-Divet L, Cornette R, Fabre AC, Herrel A & Houssaye A. **2016**. Morphological analysis of long bones in semi-aquatic mustelids and their terrestrial relatives. *Integrative and Comparative Biology* **56**: 1298–1309.
Campione NE & Evans DC. **2012**. A universal scaling relationship between body mass and proximal limb bone dimensions in quadrupedal terrestrial tetrapods. *BMC Biology* **10**: 60.
Cardini A, Polly D, Dawson R & Milne N. **2015**. Why the long face? Kangaroos and wallabies follow the same 'rule' of cranial evolutionary allometry (CREA) as placentals. *Evolutionary Biology* **42**: 169-176.
Carrano MT. **1997**. Morphological indicators of foot posture in mammals: a statistical and biomechanical analysis. *Zoological Journal of the Linnean Society* **121**: 77–104.
Cerdeño E. **1998**. Diversity and evolutionary trends of the family Rhinocerotidae (Perissodactyla). *Palaeogeography, Palaeoclimatology, Palaeoecology* **141**: 13–34.
Chen X & Tong H. **2017**. On the hindfoot bones of *Mammuthus trogontherii* from Shanshenmiaozui in Nihewan Basin, China. *Quaternary International* **445**: 50–59.
Cignoni P, Callieri M, Corsini M, Dellepiane M, Ganovelli F & Ranzuglia G. **2008**. MeshLab: an open-source mesh processing tool. *Proceedings of the 2008 Eurographics Italian Chapter Conference*: 129–136.
Coombs MC. **1982**. Chalicotheres (Perissodactyla) as large terrestrial mammals. *Third North American Paleontological Convention, Proceedings*, **I**: 99–103.**Coombs MC**. **1983**. Large mammalian clawed herbivores: a comparative study. *Transactions of the American Philosophical Society* **73**: 1–96.
Coombs MC. **1989**. Interrelationships and diversity in the Chalicotheriidae. In: Prothero DR, Schoch RM, eds. *The evolution of perissodactyls*. New York: Oxford University Press, 321–340.
Costeur L. **2004**. Cenogram analysis of the Rudabánya mammalian community: palaeoenvironmental interpretations. *Palaeontographia italica* **90**: 303.

Csuti B, Sargent EL & Bechert US. **2008**. *The elephant's foot: prevention and care of foot conditions in captive Asian and African elephants*. Ames, Iowa: John Wiley & Sons.

Curran SC. **2012**. Expanding ecomorphological methods: geometric morphometric analysis of Cervidae post-crania. *Journal of Archaeological Science* **39**: 1172–1182.

Dagosto M & Terranova CJ. **1992**. Estimating the body size of Eocene primates: a comparison of results from dental and postcranial variables. *International Journal of Primatology* **13**: 307.

Damuth, J. 1990. Problems in estimating body masses of archaic ungulates using dental measurements. In: Damuth J & MacFadden BJ, eds., *Body size in mammalian paleobiology: estimation and biological implications*. Cambridge University Press, 229-254.

DeGusta D & Vrba E. **2003**. A method for inferring paleohabitats from the functional morphology of bovid astragali. *Journal of Archaeological Science* **30**: 1009–1022.

Dinerstein E. **2011**. Family Rhinocerotidae (Rhinoceroses). In: Wilson DE, Mittermeier RA, eds. *Handbook of the mammals of the world*. Barcelona: Lynx Edicions, 144–181.

Evin A, Horáček I & Hulva P. **2011**. Phenotypic diversification and island evolution of pipistrelle bats (*Pipistrellus pipistrellus* group) in the Mediterranean region inferred from geometric morphometrics and molecular phylogenetics. *Journal of Biogeography* **38**: 2091–2105.

Fisher RE, Scott KM & Adrian B. **2010**. Hind limb myology of the common hippopotamus, *Hippopotamus amphibius* (Artiodactyla: Hippopotamidae). *Zoological Journal of the Linnean Society* **158**: 661–682.

Fortelius M & Kappelman J. **1993**. The largest land mammal ever imagined. *Zoological Journal of the Linnean Society* **108**: 85–101.

Gardezi T & da Silva J. **1999**. Diversity in relation to body size in mammals: a comparative study. *The American Naturalist* **153**: 110–123.

Gaudry M. **2017**. *Molecular phylogenetics of the rhinoceros clade and evolution of UCP1 transcriptional regulatory elements across the mammalian phylogeny*. Unpublished D. Phil. Thesis, Univeristy of Manitoba.

Geraads D, McCrossin M & Benefit B. **2012**. A new rhinoceros, *Victoriaceros kenyensis* gen. et sp. nov., and other Perissodactyla from the middle Miocene of Maboko, Kenya. *Journal of Mammalian Evolution* **19**: 57–75.

Geraads D & Spassov N. **2009**. Rhinocerotidae (Mammalia) from the late Miocene of Bulgaria. *Palaeontographica Abteilung A* **287**: 99–122.

Gladman JT, Boyer DM, Simons EL & Seiffert ER. **2013**. A calcaneus attributable to the primitive late Eocene anthropoid *Proteopithecus sylviae*: phenetic affinities and phylogenetic implications. *American Journal of Physical Anthropology* **151**: 372–397.

Gray JE. **1821**. On the natural arrangement of vertebrose animals. *London Medical Repository* **15**: 296–310.

Guérin C. **1980**. Les rhinocéros (Mammalia, Perissodactyla) du Miocène terminal au Pléistocène supérieur en Europe occidentale : comparaison avec les espèces actuelles. *Documents du Laboratoire de Géologie de la Faculté des Sciences de Lyon* **79**: 1–1182.

Guérin C. **2012**. *Anisodon grande* (Perissodactyla, Chalicotheriidae) de Sansan. *Mémoires du Muséum national d'Histoire naturelle* **203**: 279–315.

Gunz P & Mitteroecker P. **2013**. Semilandmarks: a method for quantifying curves and surfaces. *Hystrix, the Italian Journal of Mammalogy* **24**: 103–109.

Gunz P, Mitteroecker P & Bookstein FL. **2005**. Semilandmarks in three dimensions. In: Slice D, ed. *Modern morphometrics in physical anthropology*. Boston: Springer, 73–98.

Harrison JA & Manning EM. **1983**. Extreme carpal variability in *Teleoceras* (Rhinocerotidae, Mammalia). *Journal of Vertebrate Paleontology* **3**: 58–64.

Heissig K. **2012**. Les Rhinocerotidae (Perissodactyla) de Sansan. *Mémoires du Muséum national d'Histoire naturelle* **203**: 279–315.

Hildebrand M. **1982**. *Analysis of vertebrate structure*. New York: Wiley.

Hildebrand M, Bramble DM, Liem KF & Wake D. **1985**. *Functional vertebrate morphology*. Cambridge, USA: Belknap Press of Harvard University Press.

Holbrook LT & Lapergola J. **2011**. A new genus of perissodactyl (Mammalia) from the Bridgerian of Wyoming, with comments on basal perissodactyl phylogeny. *Journal of Vertebrate Paleontology* **31**: 895–901.

Houssaye A, Fernandez V & Billet G. **2016**. Hyperspecialization in some South American endemic ungulates revealed by long bone microstructure. *Journal of Mammalian Evolution* **23**: 221–235.

Jams CM, Gordon IJ & Illius AW. **1994**. Modelling equid/ruminant competition in the fossil record. *Historical Biology* **8**: 15–29.

Klingenberg CP. **1996**. Multivariate allometry. In: Marcus LF, Corti M, Loy A, Naylor GJP, Slice DE, eds. *Advances in morphometrics*. Boston, MA.

Klingenberg CP. **2016**. Size, shape, and form: concepts of allometry in geometric morphometrics. *Development Genes and Evolution* **226**: 113–137.

Knigge RP, Tocheri MW, Orr CM & McNulty KP. **2015**. Three-dimensional geometric morphometric analysis of talar morphology in extant gorilla taxa from highland and lowland habitats. *The Anatomical Record Advances in Integrative Anatomy and Evolutionary Biology* **298**: 277–290.

Lewison RL. **2011**. Family Hippopotamidae (Hippopotamuses). In: Wilson DE, Mittermeier RA, eds. *Handbook of the mammals of the world*. Barcelona: Lynx Edicions, 308-319.

MacFadden BJ. **2006**. North American Miocene land mammals from Panama. *Journal of Vertebrate Paleontology* **26**: 720–734.

Mallet C, Cornette R, Billet G, Houssaye A. 2019. Interspecific variation in the limb long bones among modern rhinoceroses—extent and drivers. PeerJ 7:e7647.

Martinez JN & Sudre J. **1995**. The astragalus of Paleogene artiodactyls: comparative morphology, variability and prediction of body mass. *Lethaia* **28**: 197–209.

Medici EP. **2011**. Family Tapiridae (Tapirs). In: Wilson DE, Mittermeier RA, eds. *Handbook of the mammals of the world*. Barcelona: Lynx Edicions, 182–203.

Missiaen P, Smith T, Guo DY, Bloch JI & Gingerich PD. **2006**. Asian gliriform origin for arctostylopid mammals. *Naturwissenschaften* **93**: 407–411.

Mitteroecker P, Gunz P, Windhager S & Schaefer K. **2013**. A brief review of shape, form, and allometry in geometric morphometrics, with applications to human facial morphology. *Hystrix, the Italian Journal of Mammalogy* **24**: 59–66.

Mitteroecker P & Gunz P. **2009**. Advances in geometric morphometrics. *Evolutionary Biology* **36**: 235–247.

Mörs T. **2002**. Biostratigraphy and paleoecology of continental Tertiary vertebrate faunas in the Lower Rhine Embayment (NW-Germany). *Netherlands Journal of Geosciences* **81**: 177–183.

Nakatsukasa M, Takai M & Setoguchi T. **1997**. Functional morphology of the postcranium and locomotor behavior of *Neosaimiri fieldsi*, a Saimiri-like Middle Miocene platyrrhine. *American Journal of Physical Anthropology* **102**: 515–544.

Osborn HF. **1923**. *Baluchitherium grangeri*, a giant hornless rhinoceros from Mongolia. *American Museum Novitates* **78**.

Osborn HF. **1929**. *The Titanotheres of ancient Wyoming, Dakota, and Nebraska*. Washington: Government Printing Office.

Owen R. **1848**. Description of teeth and portions of jaws of two extinct Anthracotherioid quadrupeds (*Hyopotamus vectianus* and *Hyop. bovinus*) discovered by the Marchioness of Hastings in the Eocene deposits on the N.W. coast of the Isle of Wight: with an attempt to

develop Cuvier's idea of the classification of pachyderms by the number of their toes. *Quarterly Journal of the Geological Society of London* **4**: 103–141.

Panciroli E, Janis C, Stockdale M & Martín-Serra A. **2017**. Correlates between calcaneal morphology and locomotion in extant and extinct carnivorous mammals. *Journal of Morphology* **278**: 1333–1353.

Paul GS & Christiansen P. **2000**. Forelimb posture in neoceratopsian dinosaurs: implications for gait and locomotion. *Paleobiology* **26**: 450–465.

Perrard A, Villemant C, Carpenter JM & Baylac M. **2012**. Differences in caste dimorphism among three hornet species (Hymenoptera: Vespidae): forewing size, shape and allometry. *Journal of Evolutionary Biology* **25**: 1389–1398.

Piras P, Maiorino L, Raia P, Marcolini F, Salvi D, Vignoli L & Kotsakis T. **2010**. Functional and phylogenetic constraints in Rhinocerotinae craniodental morphology. *Evolutionary Ecology Research* **12**: 897–928.

Plummer TW, Bishop LC & Hertel F. **2008**. Habitat preference of extant African bovids based on astragalus morphology: operationalizing ecomorphology for palaeoenvironmental reconstruction. *Journal of Archaeological Science* **35**: 3016–3027.

Polly D. **2008**. Limbs in mammalian evolution. In: Hall BK, ed. *Fins into limbs: evolution, development, and transformation*. Chicago: University of Chicago Press, 245–268.

Prothero DR. **2005**. Biogeography and diversity patterns. In: *The evolution of North American rhinoceroses*. Cambridge: Cambridge University Press, 182-199.

Prothero DR. **2013**. *Rhinoceros giants: the paleobiology of indricotheres*. Bloomington: Indiana University Press.

Prothero DR, Guérin C & Manning E. **1989**. The history of the Rhinocerotoidea. In: Prothero DR, Schoch RM, eds. *The evolution of perissodactyls*. New York: Oxford University Press, 321–340.

Prothero DR & Schoch RM (Eds.). **1989**. *The evolution of perissodactyls*. New York: Oxford University Press.

R Development Core Team. **2005**. *R: A language and environment for statistical computing*. Vienna, Austria: R Foundation for Statistical Computing.

RStudio, Inc. 2018. *RStudio*. Boston, MA.

Rubenstein DI. **2011**. Family Equidae (Horses and relatives). In: Wilson DE, Mittermeier RA, eds. *Handbook of the mammals of the world*. Barcelona: Lynx Edicions, 106–143.

Saarinen J, Eronen J, Fortelius M, Seppä H & Lister A. **2016**. Patterns of diet and body mass of large ungulates from the Pleistocene of Western Europe, and their relation to vegetation. *Palaeontologia Electronica* **19**: 1–58.

Scarborough ME, Palombo MR & Chinsamy A. **2016**. Insular adaptations in the astragalus-calcaneus of Sicilian and Maltese dwarf elephants. *Quaternary International* **406**: 111–122.

Schlager S, Jefferis G & Dryden I. **2018**. *Morpho: a toolbox providing methods for data-acquisition, visualisation and statistical methods related to Geometric Morphometrics and shape analysis*.

Schulz-Kornas E, J. M F, Merceron G & Kaiser T. **2007**. Feeding ecology of the Chalicotheriidae (Mammalia, Perissodactyla, Ancylopoda). Results from dental micro- and mesowear analyses. *Verhandlungen des Naturwissenschaftlichen Vereins zu Hamburg* **43**: 5–32.

Semprebon GM, Sise PJ & Coombs MC. **2011**. Potential bark and fruit browsing as revealed by stereomicrowear analysis of the peculiar clawed herbivores known as chalicotheres (Perissodactyla, Chalicotherioidea). *Journal of Mammalian Evolution* **18**: 33–55.

Shockey B & Anaya Daza F. **2004**. *Pyrotherium macfaddeni*, sp nov (Late Oligocene, Bolivia) and the pedal morphology of pyrotheres. *Journal of Vertebrate Paleontology* **24**: 481–488.

Stains HJ. **1959**. Use of the calcaneum in studies of taxonomy and food habits. *Journal of Mammalogy* **40**: 392–401.

Steiner CC & Ryder OA. **2011**. Molecular phylogeny and evolution of the Perissodactyla: phylogeny of the perissodactyls. *Zoological Journal of the Linnean Society* **163**: 1289–1303.

Tsubamoto T. **2014**. Estimating body mass from the astragalus in mammals. *Acta Palaeontologica Polonica* **59**: 259–265.

Valli AM. **2005**. Taphonomy of the late Miocene mammal locality of Akkasdagı, Turkey. *Geodiversitas* **27**.

Wall WP. **1989**. The phylogenetic history and adaptive radiation of Amynodontidae. In: Prothero DR, Schoch RM, eds. *The evolution of perissodactyls*. New York: Oxford University Press, 341–354.

Wang H, Bai B, Meng J & Wang Y. **2016**. Earliest known unequivocal rhinocerotoid sheds new light on the origin of giant rhinos and phylogeny of early rhinocerotoids. *Scientific Reports* **6**.

White TD & Folkens PA. **2005**. Chapter 16 - Foot: tarsals, metatarsals, & phalanges. In: White TD, Folkens PA, eds. *The Human bone manual*. San Diego: Academic Press, 287–308.
Wiley DF. **2005**. *Landmark*. Institute for data analysis and visualization.
Willerslev E, Gilbert MTP, Binladen J, Ho SY, Campos PF, Ratan A, Tomsho LP, da Fonseca RR, Sher A, Kuznetsova TV, Nowak-Kemp M, Roth TL, Miller W & Schuster SC. **2009**. Analysis of complete mitochondrial genomes from extinct and extant rhinoceroses reveals lack of phylogenetic resolution. *BMC Evolutionary Biology* **9**: 95.
Zapfe H. **1979**. *Chalicotherium grande (BLAINV.) aus der miozänen Spaltenfüllung von Neudorf an der March (Děvinská Nová Ves), Tschechoslowakei*. Berger.
Zhegallo V, Kalandadze N, Shapovalov A, Bessudnova Z, Noskova N & Tesakova E. **2005**. On the fossil rhinoceros *Elasmotherium* (including the collections of the Russian Academy of Sciences). *Cranium* **22**: 17–40.

Supporting Information

Additional Supporting Information may be found in the online version of this article at the publisher's web-site.

Appendix 1. List of all the specimens studied.

Appendix 2. Anatomical description of the bones.

Appendix 3. Description of the landmarks and curves placed on the bones.

Appendix 4. Results of the repeatability tests.

Appendix 5. Correlation between centroid size and mean body mass.

Appendix 6. Results of the K-mult test.

Appendix 7. Vector representations of all the shape variations described in the article.

Fig. S1. Right astragalus of *Rhinoceros unicornis* MNHN-ZM-AC-1960-59, in A: anterior, B: lateral, C: posterior and D: distal views. **LR**: lateral ridge of the trochlea, **MR**: medial ridge of the trochlea, **G**: groove of the trochlea, **Tr**: trochlea, **F TM**: facet for the tibial malleolus, **F FM**: facet for the fibular malleolus, **F N**: facet for the navicular, **F Cu**: facet for the cuboid, **PF C**: posterior facet for the calcaneus, **MF C**: medial facet for the calcaneus, **DF C**: distal facet for the calcaneus, **M T**: medial tubercle, **P T**: posterior tubercle.

Fig. S2. Right calcaneus of *Ceratotherium simum* MNHN-ZM-MO-2005-297, in A: anterior, B: medial, and C: distal views. **TUBER**: Tuber calcanei, **HEAD**: head of the calcaneus, **ST**: sustentaculum tali, **RC**: rostrum calcanei, **GA**: great apophysis, **MF A**: medial facet for the astragalus, **PF A**: proximal facet for the astragalus, **DF A**: distal facet for the astragalus, **F Cu**: facet for the cuboid, **L T**: lateral tubercle.

Fig. S3. Results of the PCA with 10 replicates of the landmarks on three different but morphologically close individuals, for each bone.

Fig. S4. Regression plot of the logarithm of the centroid size of each individual against the logarithm of the cubic root of the mean mass of its species, for both bones and for both the Rhinocerotidae and Perissodactyla dataset.

Fig. S5. A. Vector representations of the shape variations on PC1, PC2 and PC4 on the analysis on the astragalus of Rhinocerotidae. Posterior view. **B.** Left: vector representations of the shape corresponding to theoretical minimum and maximum of allometry on the astragalus of Rhinocerotidae. Right: vector representations of the shape corresponding to theoretical minimum and maximum of mass on allometry-free shapes on the astragalus of Rhinocerotidae. Posterior view. **C.** Vector representations of the shape variations on PC1 and PC2 on the analysis on the calcaneus of Rhinocerotidae. Antero-medial view. **D.** Left: vector representations of the shape corresponding to theoretical minimum and maximum of allometry on the calcaneus of Rhinocerotidae. Right: vector representations of the shape corresponding to theoretical minimum and maximum of mass on allometry-free shapes on the calcaneus of Rhinocerotidae. Antero-medial view. **E.** Vector representations of the shape variations on PC1, PC2 and PC3 on the analysis on the astragalus of Perissodactyla. Posterior view. **F.** Left: vector representations of the shape corresponding to theoretical minimum and maximum of allometry on the astragalus of Perissodactyla. Right: vector representations of the shape corresponding to theoretical minimum and maximum of mass on allometry-free shapes on the astragalus of Perissodactyla. Posterior view. **G.** Vector representations of the shape variations on PC1 and PC2 on the analysis on the calcaneus of Perissodactyla. Antero-medial view. **H.** Left: vector representations of the shape corresponding to theoretical minimum and maximum of allometry on the calcaneus of Perissodactyla. Right: vector representations of the shape corresponding to theoretical minimum and maximum of mass on allometry-free shapes on the calcaneus of Perissodactyla. Antero-medial view.